Central Washington University

# ScholarWorks@CWU

Spring 2022

# Binding Interactions Between Mixed-Monlayer Functionalized Gold Nanoparticles (AuNPs) And the Serum Protein Albumin

Jennifer Hanigan-Diebel
*Central Washington University*

Follow this and additional works at: https://digitalcommons.cwu.edu/etd

Part of the Other Chemistry Commons

## Recommended Citation

Hanigan-Diebel, Jennifer, "Binding Interactions Between Mixed-Monlayer Functionalized Gold Nanoparticles (AuNPs) And the Serum Protein Albumin" (2022). *All Master's Theses*. 1778.
https://digitalcommons.cwu.edu/etd/1778

BINDING INTERACTIONS BETWEEN MIXED-MONLAYER FUNCTIONALIZED GOLD

NANOPARTICLES (AuNPs) AND THE SERUM PROTEIN ALBUMIN

_____

A Thesis

Presented to

The Graduate Faculty

Central Washington University

_____

In Partial Fulfillment

of the Requirements for the Degree

Master of Science

Chemistry

_____

by

Jennifer Lynn Hanigan-Diebel

May 2022

CENTRAL WASHINGTON UNIVERSITY

Graduate Studies

We hereby approve the thesis of

Jennifer Lynn Hanigan-Diebel

Candidate for the degree of Master of Science

APPROVED FOR THE GRADUATE FACULTY

_____        _____

                              Dr. Sam Lohse, Committee Chair

_____        _____

                              Dr. Carin Thomas-Bradley

_____        _____

                              Dr. Yingbin Ge

_____        _____

                              Dean of Graduate Studies

ABSTRACT

This study investigated the protein adsorption interactions of bovine serum albumin (BSA) with three different functionalized 5 nm gold nanoparticles (AuNPs) in order to determine the binding affinity and total amount of protein adsorbed to each AuNP surface chemistry. AuNPs were synthesized using two different capping agents to display three different surface chemistries: a neutral ω-functionalized thiol ligand (mercapto-ethoxy-ethoxy-ethanol, MEEE), a thiol ligand that is negatively charged at pH 7.4 (mercaptohexanoic acid, MHA), and a mixture of the two ligands (mixed-ligand AuNPs). The interactions of this library of AuNPs with bovine serum albumin (BSA) were investigated using UV-visible absorbance spectroscopy, fluorescence titrations, dynamic light scattering (DLS), and a Bradford protein assay. Fluorescence titrations indicated that the binding affinity of BSA was higher for AuNPs with any negative surface charge density, and that the difference between $K_a$s for the mixed-ligand AuNPs and the MHA-capped AuNPs was not significant. $K_a$ for MHA, MEEE, and mixed-ligand AuNPs were $0.47 \pm 0.02$ nM$^{-1}$, $0.40 \pm 0.02$ nM$^{-1}$, and $0.48 \pm 0.02$ nM$^{-1}$, respectively. Hill plot analysis of the fluorescence titration data indicated that for all three AuNP surface chemistries, BSA exhibited cooperative binding behavior. Measurement of the hydrodynamic diameter (Dh) by dynamic light scattering (DLS) suggests that 1 to 2 BSA molecules adsorb to each AuNP, but quantitation of the total protein adsorbed to each AuNP surface chemistry was not possible via Bradford assay due to an inability to adequately separate BSA-AuNP complexes from free BSA.

ACKNOWLEDGMENTS

This research was inspired and guided by Dr. Sam Lohse, to whom I owe a heap of gratitude.  I've truly enjoyed working with you.  Thank you.

Dr. Carin Thomas-Bradley and Dr. Yingbin Ge, thank you for your hours upon hours of teaching, and your willingness to serve on my committee.

Dr. Eric Melby, thank you for giving me a foundation in chemistry and in so much more, and for being proud of me.

I owe so much to the Graduate Committee of the CWU Chemistry Department for their award of the Ivory Nelson Fellowship, which enabled me to dedicate a summer to research.  And to all the faculty and staff, thank you for creating an environment of learning, connection, and joy.

To Matthias Carroll, my fellow researcher, many thanks for your help and just as many wishes for your future success.  Thanks also to Bethany Eaton and Keith Chlebik, with whom I shared not just an office but a whole journey.

On a personal note, I also owe countless thanks to:

My parents, Richard Diebel, Noël Egert, and Debra Hanigan, for believing in me and encouraging me with your words and your pocketbooks.

Nathan Moore, for the hours of calculus and physics tutoring, the supply runs, and the tech support. You're an incredible human and I'm blessed to be your mother.

Crystal Conner, sister of my heart and best aunt my cat could ever wish for, for putting up with the stacks of books and papers where the dining room table ought to have been, for all the late night talks and nuggets of wisdom, and for making my life more beautiful.

My grandparents, Olinda Diebel and Norman Diebel, who filled my childhood with books. Grandpa, I wish you could have read this—you'd have understood it.

Judith Johannesen for her support and encouragement. It seems I won't be needing that career in stand-up comedy after all.

Sara Michaels Stewart for the many hours of co-working companionship.

And finally, Dr. Nancy R. Goodloe, partner, cheerleader, coach—you remain the happiest of surprises. Thank you.

TABLE OF CONTENTS

LIST OF FIGURES

LIST OF FIGURES (CONTINUED)

LIST OF FIGURES (CONTINUED)

CHAPTER I

INTRODUCTION

Engineered nanoparticles (ENPs) are usually defined as materials (metals, semiconductors, polymers, etc.) having at least one dimension under 100 nm.  Most ENPs are synthesized with a two-part structure consisting of a core of inorganic material and an organic capping agent bound to the core's surface (Figure 1).
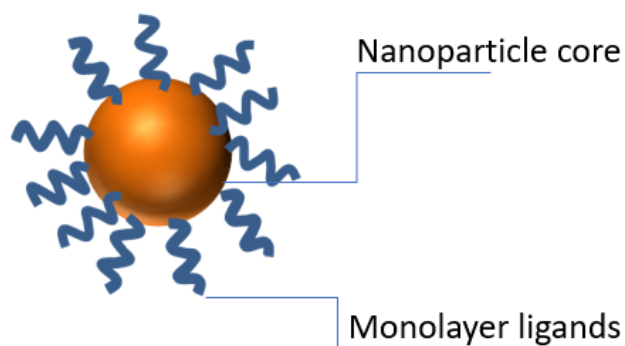


Figure 1.  Simplified diagram of an engineered nanoparticle.

The core material provides the ENP with its size-dependent properties.  Due to the unique size regime and high surface curvature, these properties differ from that of their bulk material counterparts.  For instance, gold nanoparticles (AuNPs) in solution appear red to purple depending on core size, rather than the characteristic gold color associated with the bulk material.[1]  AuNPs can also convert light into localized heat, making them useful for photothermal therapy.  Tumor cells accumulate a build-up of AuNPs at a higher rate than the surrounding healthy tissue, allowing them to be excited by light trans dermally.  The heat given off by the excited AuNPs kills the tumor tissue.[2]

Researchers have also used AuNPs bonded to a titanium dioxide substrate to catalyze the splitting of $H_2$ at room temperature by exciting electrons in the AuNP plasmon with a laser, creating electron-hole pairs.  The excited electrons provide the catalytic function needed without the high temperatures required in other processes.[3]

To preserve the size-dependent properties, ENPs dispersed in solution must have a capping agent present on the surface.  The capping agent layer consists of either a monolayer of organic molecules bound to the surface of the core material or an inorganic shell such as silicon dioxide ($SiO_2$).  This capping agent, by steric hindrance and/or electrostatic repulsion, provides a physical barrier between ENP cores.  The capping agent also functions as the interface between the ENP and its environment. The capping agent's chemical composition directs the interactions between the ENP and its surroundings to a great extent, in concert with the ENP's core size and composition.[4,5]  The wide variety of core compositions, core sizes, and capping agent (surface chemistry) choices results in a sizeable catalog of possible ENPs, each with its own physiochemical properties.

The physiochemical properties of nanomaterials are controlled through their synthesis.  ENPs can be synthesized using a wide variety of methods, including in-solution synthesis (redox or polymerization reactions) and mechanical methods (such as laser ablation).[1]  Metal core NPs, including AuNPs, are typically synthesized *via* a direct synthesis such as the reduction of chloroauric acid ($HAuCl_4$) by a mild reducing agent such as sodium borohydride ($NaBH_4$).[6]

Because ENPs are complex chemical systems whose properties and behaviors depend on both the size (and shape) of the NP's core and the chemical composition of molecules on its surface, effective characterization of all the NP physiochemical properties is necessary for any study of NP behavior.

NP core size ($d_{core}$) can be characterized by electron microscopy (EM), although EM is not useful for determining the total diameter of the NP with an organic capping agent layer included. This overall diameter (the hydrodynamic diameter, $D_h$) is better characterized *via* dynamic light scattering (DLS).  When the core consists of a plasmonic metal like gold, capable of creating an oscillating field of free electrons under certain circumstances, UV-visible absorbance spectroscopy can also be used to characterize the core diameter.[7]  This provides a quick, non-destructive method of determining core diameter during synthesis.

The composition and structure of the organic capping agent, both before and after nanoparticle synthesis, can be investigated *via* proton NMR spectroscopy (^{1}H-NMR).  ^{1}H-NMR spectroscopy is a technique which uses a magnetic field and radio waves to determine the chemical environment of the hydrogen atoms in an organic molecule.  Hydrogen atoms appear as peaks on the spectra with the peak location determined by the hydrogen atom's chemical environment (what other atoms or groups of atoms it is close to), and peak area is determined by the number of hydrogen atoms that share an identical chemical environment.  The structure of the molecule can be extrapolated from the spectra.[6]

Like most xenobiotics, nanoparticles in the bloodstream associate with endogenous proteins, such as the very abundant serum albumin. These nanoparticle-protein associations change with the variations in the size, core composition, and surface chemistry of the nanoparticles, and in many cases have not yet been fully elucidated.[8] The effect of surface chemistry on these interactions can be investigated through studies of NPs with the same core composition and diameter, but differing surface chemistry.

One measure of AuNP-protein interactions is binding affinity. The binding affinity of bovine serum albumin (BSA) for gold nanoparticles (AuNPs) can be measured with a fluorescence quenching titration. Fluorescence titration, a fluorescence spectroscopy technique wherein the fluorophore concentration is held constant while the quencher concentration is varied, will provide a linear relationship between quencher concentration and fluorescence if the quenching is due to stable fluorophore-quencher interactions (static quenching). BSA contains intrinsically fluorescent tryptophan residues ($\lambda_{ex}$ = 280 nm, $\lambda_{em}$ = 350 nm), that is, when they are exposed to light at a certain wavelength they in turn give off light at a different wavelength. This fluorescence is quenched when the fluorophore is within 10 nm of a quencher, such as the surface of a gold nanoparticle.[9] Therefore, binding by BSA to the AuNP surface results in a loss of the tryptophan residue's fluorescence signal. Fluorescence titration is also useful for determining if the binding of proteins onto the nanoparticle is cooperative or not. When cooperative binding is present, the binding of one molecule

4

of protein to a NP increases the chances of additional protein molecules binding, and this is evidenced by the slope of the line applied to a double logarithmic plot of the fluorescence data.[9]

In addition to binding affinity, it can be useful to quantitate the total amount of protein bound to a nanoparticle.  For low concentrations of protein (e.g. 2-3000 µg/mL) this can be done *via* a Bradford assay.  The Bradford reagent (Coomassie Brilliant Blue G-250), which appears red in a methanol solution, binds to basic and aromatic residues in proteins and, in this bound state, changes color to blue, absorbing light at a wavelength of 595 nm.[10]  The relationship between the concentration of protein and this absorption is linear in accordance with the Beer-Lambert Law, up to approximately 3000 µg/mL.  As with pure NPs dispersed in solution, the $D_h$ of NPs with adsorbed BSA can be measured with DLS to determine the increase in diameter due to the adsorbed protein.

CHAPTER II

LITERATURE REVIEW

The size and nanoscale properties of engineered nanoparticles make them ideal

candidates for *in vivo* usage as both diagnostic and therapeutic agents.  As a result of

their particular size regime (100 nm or less), NPs are capable of interacting in unique

ways with individual biological molecules.[1]  The specific size-dependent properties that

NPs manifest are governed by the composition and size of the core material, and can be

leveraged for applications in ways that molecular pharmaceuticals and imaging agents

cannot.[2,11]  For instance, NPs synthesized with gold or silver cores exhibit surface

plasmons.  The surface plasmon is an oscillating field of delocalized electrons that

provides unique light scattering and photothermal properties to the NPs which can be

leveraged for theranostic applications.  Theranostic agents combine enhanced

sensitivity diagnostic capabilities with therapeutic functions in the same material.[11]

The optical properties of gold nanoparticles (AuNPs), in particular, can be

exploited for extreme sensitivity in imaging applications.  Vickers, et al., for example,

compared the two-photon photoluminescence properties of hollow gold nanospheres

(HGNs) and gold nanorods (AuNRs).[2]  Two-photon photoluminescence involves directing

two low-energy photon sources at the photoluminescent target such that the combined

energy reaches the level needed to excite the target.  The low-energy photons are

capable of penetrating tissue that higher-energy photons would not pass through.  Thus,

when administered *in vivo*, the photoluminescent and photothermal properties of HGNs

and GNRs can be used to provide both imaging and targeted thermal destruction of

tumor cells.  The photothermal efficiency of NPs varies with the size, shape, and core

material.  Cole et al. compared the photothermal efficiencies of Au nanorods and

Au/SiO$_2$ and Au/Au$_2$S nanoshells, and determined that the efficiency varied such that it

would be possible to tune the size and shape of NPs during synthesis to yield the desired

result, balancing transduction efficiency and the quantity of NPs needed.[12]

Sokolov et al. investigated the use of AuNPs in the imaging of live tissue.

Researchers conjugated monoclonal antibodies for epidermal growth factor receptor

(EGFR), a transmembrane protein overexpressed by precancerous epithelial cells, to

AuNPs of 12 nm diameter.  When applied topically to live tissue using a penetration

enhancer, the monoclonal antibodies bound to the precancerous cells and the

conjugated AuNPs enabled visualization with reflectance microscopy.  The hope is that

this can be performed endoscopically, eliminating the need for biopsies as a screening

method, and providing the needed screenings at low cost.[13]

*In vivo* applications of ENPs are complicated by the formation of the protein

corona (PC), an irreversible shell of proteins that adsorb to the NP as soon as it enters

the bloodstream.  The PC becomes the new biological identity of the NP, dictating (for

better or worse) its interactions with its surroundings.  The formation of the NP's PC is

driven by a variety of intermolecular interactions, including Van der Waals forces,

hydrogen bonding, electrostatic forces, and hydrophobic interactions.[14] The dominant

intermolecular forces depend on the NP's physiochemical characteristics (primarily size and surface chemistry), although electrostatic interactions are believed to be pivotal.[14] Understanding, preventing, and directing PC formation is thus the goal of much research, as will be discussed here.

Some research groups have investigated the impact of NP core size on PC formation. Piella et al. studied citrate-capped AuNPs ranging in size from 3.5 nm to 150 nm. For the smallest AuNPs, which are smaller than the serum proteins with which they interacted, the PC remained loosely and incompletely formed. As the NP core size became larger, PC formation became dense and irreversible, and for the largest particles, a multi-layer PC was observed.[15] Partikel et al. looked at 100 nm and 200 nm polymer NPs, which they incubated with fetal bovine serum (FBS). They were unable to find any size-dependent effect on the quantity of adsorbed protein as measured by a Bradford assay, but they did determine that modifying the surface of their NPs with poly(ethylene) glycol (PEG) reduced protein adsorption.[5]

PEGylation is frequently used when engineering NPs to mitigate protein adsorption. Wang et al. studied the impact of surface chemistry on PC formation by synthesizing 13 nm AuNPs passivated with citrate, cysteine, CTAB, or PEG (of molecular weights of either 2kDa or 5kDa) and incubated them with bovine serum albumin (BSA). PC formation was measured by a variety of methods including fluorescence spectroscopy and dynamic light scattering (DLS). The researchers found that 5k

PEGylation prevented protein adsorption, and that, in general, the quantity of adsorbed protein increased with AuNP surface charge.[16]

While PEGylation works to prevent protein adsorption, Larson et al. showed that for AuNPs the thiol bond between the capping ligand and the gold core is susceptible to displacement by sulfur-containing endogenous molecules such as cysteine and cystine. To prevent this, they added an alkyl chain to the capping ligands between the sulfur and PEG ends. The hydrophobic interactions between the alkyl chains on neighboring ligands formed a shield against the penetration of endogenous molecules to the core, preventing ligand displacement. They also found that these measures correlated with reduced macrophage uptake.[17]

The development of successful ENP theranostics is not as simple as the prevention of PC formation and macrophage uptake. To effectively target specific biomolecules, the nano-bio interactions must be more finely controlled and anticipated in the design of the NP therapeutics. Walkey et al. developed a model to predict nano-bio interactions. First, they synthesized a library of 105 types of gold AuNPs in 15, 30, and 60 nm core diameter sizes with a variety of monolayer ligands categorized as neutral, anionic, and cationic at pH 7.4 (the physiological pH of blood). After synthesis and characterization by dynamic light scattering, absorbance spectroscopy, and agarose gel electrophoresis, the AuNPs were incubated for one hour with undiluted human serum at 37 °C. Post-incubation the AuNPs were separated by centrifugation along with any protein coronas which had formed. The makeup of these protein coronas was

then assessed via polyacrylamide gel electrophoresis (PAGE), LC-MS/MS, and western blot. The results showed that the protein coronas formed on each AuNP type were composed of a ratio of proteins that differed from the ratio of abundance in the serum and which was unique to each nanoparticle type, indicating that the character of the nanoparticle (both the size and ligand functionality) influenced which individual proteins adsorbed to it. The resulting protein composition is therefore a "fingerprint" unique to the nanoparticle type. The researchers then developed a model to predict cell interactions based on the protein corona fingerprint and determined that, for nanoparticles in the 15-60 nm core diameter range, both the ligand and the size influenced formation of the corona and subsequent cell interactions, the former more heavily than the latter. The researchers also tested a smaller library of silver nanoparticles and determined that the core material used impacts the corona such that the fingerprint model developed using gold nanoparticles could not be applied to silver nanoparticles.[18]

The PC fingerprint findings suggest protein-protein interactions greatly influence PC formation. In other words, the proteins that adsorb to the NP surface first set the template for the subsequent adsorption of proteins to the NP. To investigate the role of protein-protein interactions in PC formation, Zhang et al. synthesized citrate-capped 60 nm AuNPs, which they then incubated with human serum. LC-MS/MS was used to identify the protein makeup of the PC that formed during incubation. The researchers tested the binding functionality of 24 of the protein types contained in the PC with an

enzyme-linked immunosorbent assay (ELISA).  Proteins that retain their binding

functionality will bind to the antibody used in the assay.  Only 27.4% of the total

proteins demonstrated functionality in the ELISA assay, indicating that either they

underwent a conformational change that prevented binding, or they were encased in a

multi-layer corona.  This held true even when the gold core was removed with diiodine

etching.  They were also able to determine which proteins bound to one another,

indicating that the final composition of the PC can be manipulated if the proteins

adsorbed initially can be controlled, such as by pre-coating the NPs.[19]

For some theranostic applications, cellular uptake of ENPs is desired.  NPs enter

cells *via* multiple endocytic routes, and uptake tends to be efficient, leading some to

hope that conjugating ENPs with drug molecules that would otherwise be unable to pass

through the cell wall may aid in drug delivery.  It is commonly seen, however, that ENPs

remain confined to endosomes after uptake, preventing them from reaching their

desired target.[20]  Connor et al. tested 4, 12, and 18 nm AuNPs capped with cysteine,

citrate, biotin, and cetyltrimethylammonium bromide (CTAB) for cytotoxicity using

leukemia cells.  They determined that all AuNPs were taken up into cells but this did not

result in toxicity.  This result is interesting since CTAB itself is known to be toxic, but

once bound to the AuNP no toxic effects were seen.  The researchers suggested that

much further research be done given the large variety of ENPs available.[21]  Murphy et al.

assessed the interactions of virus-sized (up to 10 x 100 nm) gold nanorods (AuNRs) and

AuNPs with biological systems.  Both chronic and acute exposure tests were performed

with neither showing an effect on cell viability.  The researchers found that acute exposure resulted in cell stress that could be detected 20 weeks later, but chronic exposure resulted in adaptive behavior by the cells to mitigate the stress.[11]

Cell stress is only one measure of possible toxicity.  Given the ENP-protein and protein-protein interactions, there is some concern about ENP-instigated protein misfolding, which can induce disease states.  Dominguez-Medina et al. investigated this possibility using mercaptoundecyltrimethylammonium bromide (MUTAB) coated AuNRs and BSA, and found that, at least at low protein concentrations, a single protein adsorbs irreversibly, unfolds, and due to its unfolded state drives further protein-protein interactions, which in turn drives nanoparticle aggregation, an undesirable outcome.[22] And Chakraborty et al. investigated interactions of BSA with CTAB-capped 8 x 20 nm GNRs and 3-4 nm AuNPs.  They found that the GNRs induced BSA aggregation by causing misfolding, and the misfolded proteins interacted with other protein molecules.  Unlike the GNRs, the AuNPs did not cause these conformational changes in the BSA molecules. They also found that the binding of BSA to AuNPs is exothermic in nature but with GNRs it is endothermic and entropically driven by a release of water from the hydrophobic site of BSA upon binding.[23]  Shi et al., however, did find conformational changes when studying the interactions of BSA with 13.9 nm citrate-capped AuNPs.[24]

While a wide variety of materials are appropriate in nanoparticle cores chosen for theranostic applications, wherein diagnostic and therapeutic capabilities are combined in the same platform, gold is especially useful for these purposes.[14]  Its low

toxicity (in bulk) and photothermal and photoluminescent properties lend themselves to

*in vitro* use and a variety of assay techniques.[14]  AuNPs in a variety of sizes and shapes

can also be synthesized conveniently (generally rapidly, in water, at room temperature)

in a direct synthesis, making AuNPs convenient model nanoparticles for investigating

protein-ENP interactions (*vide supra*). The strong light-absorbing and scattering

properties of AuNPs also means that AuNP-serum protein interactions can be studied

using a variety of spectroscopic methods such as absorbance spectroscopy, fluorescence

spectroscopy, and dynamic light scattering.

The Brust-Shiffrin reaction, published in 1994, involved a two-step process for

AuNP synthesis.  First, chloroauric acid was mixed with ligands that terminate in a thiol

functional group.  This complex is then reduced with sodium borohydride ($NaBH_4$).[6]

Bunte salts (alkylthiosulfates) can be used in place of thiols to access a wider range of

core sizes and generate particles with a mixture of two ligands in the capping agent

layer.[6,25,26]  During this synthesis, the ligands form a thiol bond to the gold, eliminating a

sulfite group in the process, which functioned as a type of protecting group up until that

point.  Because AuNP formation involves nucleation-growth-passivation kinetics, the

slower bonding by the Bunte salts yields larger AuNPs.[25]  For additional control of AuNP

core size, Elliott et al. developed a relationship between the pH of the reaction solutions

and the final core size.  As pH rises so does core size, between 2 and 9 nm along a

polynomial curve.[26]  Bunte salts themselves can be synthesized from organohalides and

sodium thiosulfate.[25]  The organohalide precursors can be functionalized in a variety of

ways, and in combination with size-selection during synthesis, an extremely wide variety of functionalized AuNPs can be produced.

While investigation of nanoparticles and nano-bio interactions has received a great deal of attention, the bulk of the studies, as reflected in this review, have involved ENPs with core diameters of 15-200 nm. A great deal of research has been done on the relationship between different surface chemistries and PC formation, but few studies found during this review have investigated the impact of subtler changes in surface chemistry such as that brought about by mixing monolayer ligands of differing types. The studies herein leverage the direct synthesis process discussed above, utilizing Bunte salt ligand precursors of two types: mercaptohexanoic acid (MHA) and mercaptoethoxyethoxy ethanol (MEEE). The former thiol (containing a carboxylic acid ω-functionality) is negatively charged at pH 7.4, while the latter thiol (a short-chain PEG) is neutral at all solution pHs. The direct synthesis process also allows for the mixing of both thiol ligands on the surface of the AuNP, resulting in AuNPs with surface charge densities intermediate between the completely negatively charged case and the completely neutral-case. Additionally, the process allows for a targeted NP core diameter of 5 nm, resulting in NPs that are the same size as the model protein used (BSA).

In the experimental work that follows, 5 nm AuNPs stabilized with MHA, MEEE, or mixed MEEE:MHA ligands were synthesized, characterized, and used to investigate the binding interactions between the AuNPs and the model protein BSA. BSA, the most

abundant serum protein, is similar in size (MW = 67 kDa, $D_h \sim 7$ nm) to the AuNPs being investigated.  The interactions of the three AuNP types with BSA, including the stability of the AuNP-BSA conjugates in saline, binding constants ($K_a$), and the total amount of BSA adsorbed by each AuNP, were investigated and the results compared to determine how and to what extent mixing the monolayer ligands impacts the BSA-AuNP interactions.

CHAPTER III

METHODS AND MATERIALS

*Materials*

Hydrogen tetrachloroaurate trihydrate (HAuCl$_4$·3H$_2$O) was obtained from Aldrich

and sodium borohydride (NaBH$_4$) was obtained from Sigma Aldrich, all used as received.

Sodium hydroxide (NaOH) was used as received.  6-bromohexanoic acid (97%) and 2-[2-

(2-chloroethoxy)ethoxy] ethanol (97%), bovine serum albumin (>98%, Sigma), sodium

chloride (>99%) were obtained from Sigma Aldrich and used as received.  Sodium

bicarbonate buffer was prepared from sodium bicarbonate solid and buffer pH was

adjusted by addition of HCl.  Bradford reagent (Coomassie Brilliant Blue) was obtained

from Bio-Rad and used as received.  MilliQ deionized water (18 MΩ) was used as a

solvent in all stock solution preparations.  Measurements of pH performed with Mettler-

Toldeo, SG23 handheld pH meter.  Absorbance spectra were taken using an Agilent

8543 UV-Visible spectrophotometer.  Dynamic light scattering (DLS) was performed

using a Malvern MasterSizer 3000.  NMR was performed on a Bruker 400 MHz NMR.

Fluorescence spectroscopy was performed on a Horiba FluoroMax fluorometer.

Fluorescence cuvettes used were from Alpha Nanotech.  Microchannel cuvettes used for

UV-visible absorbance spectroscopy were obtained from Starna.  Pall Tangential flow

filtration cassettes (diafiltration, 10 kDa) were obtained from VWR.

*Bunte Salt Preparation*

Bunte salt ligand precursors were synthesized according to previously published methods.[25]  Briefly, organohalide precursors (2-[2-(2-chloroethoxy)ethoxy] ethanol (for MEEE) or 6-bromohexanoic acid (for MHA) and sodium thiosulfate ($Na_2S_2O_3$) in a 1:0.8 molar ratio were mixed a 50:50 solution of MilliQ $H_2O$ and ethanol and refluxed for at least 4 hours.  The water and ethanol were removed by rotary evaporation.  The crude product was redissolved in ethanol and gravity filtered.  Then the ethanol was removed once again by rotary evaporation followed by overnight drying in a vacuum oven.  Formation of the functionalized Bunte salts was verified by ^{1}H-NMR spectroscopy ($D_2O$, 400 MHz).

*AuNP Synthesis and Purification*

AuNPs were synthesized according to previously published methods.[25,26]  Briefly, 5 molar equivalents of  $HAuCl_4$ were mixed with 2 molar equivalents of functionalized Bunte salts (either MEEE, MHA, or, for the mixed-ligand AuNPs, a 90:10 ratio of MEEE to MHA) in water and stirred with magnetic stir bar and plate for 5 minutes.  Two molar equivalents of aqueous $NaBH_4$ were then added to the $HAuCl_4$ solution and stirring continued.  Desired AuNP core sizes were achieved by adjusting pH of both solutions with small amounts of 1 M NaOH, and by adjusting concentrations of Bunte salts used.

AuNPs were purified via diafiltration.[25]  First, the crude AuNP solution was reduced to an initial volume of 15 mL in the diafiltration apparatus.  Then, MilliQ water

was added to the AuNP solution as diafiltration continued until 300 mL of total filtrate volume had been passed through the system.  The purified AuNP solution was then concentrated to a volume of 25 mL.

*AuNP Characterization*

Core size and AuNP concentration were determined via UV-visible absorbance spectroscopy according to previously published methods.[7]  The hydrodynamic diameter ($D_h$) of the AuNPs in solution was determined by dynamic light scattering (DLS). The surface composition of the ligands on the purified nanoparticle was determined by proton $^1$H-NMR spectroscopy ($D_2O$, 400 MHz) after digesting the AuNPs with diiodide by addition of solid diiodide to the NMR tubes containing the sample.

*Transmission Electron Microscopy*

Transmission electron microscopy (TEM) images of the particles were obtained using a Thermo FEI Tecnai G2 Spirit Transmission Electron Microscope operated at 300 kV. Aqueous solutions of AuNPs were drop cast directly onto Cu/SiO TEM grids (PELCO) for imaging.  ImageJ software was used to analyze the TEM images.

*Dynamic Light Scattering*

Aqueous samples of each AuNP type were prepared for dynamic light scattering analysis in MilliQ water or 105 mM NaCl at pH 7.4 with 0.25 mg/mL BSA.  The AuNP concentration for each sample was 5 nM and the total sample volume was 3 mL for each.   MilliQ water was used as the dispersant for all samples.

*Stability Studies*

5 nm MHA- and MEEE-capped AuNPs were incubated in 1 mM, 10 mM, and 100 mM NaCl solutions at pH 7.4 at 37 °C. The AuNP concentration was 5.0 nM in all incubation trials.  UV-visible absorbance spectra of the AuNP solutions were taken immediately after mixing and at 15, 30, and 60 minutes, and spectra of each AuNP sample suspended in water without NaCl or buffer were also taken.  MHA- and MEEE-AuNPs were also incubated with 30 mg/mL and 60 mg/mL BSA at 105 mM NaCl at pH 7.4 for 60 minutes at 37 °C.  UV-visible absorbance spectra of the BSA-AuNP conjugate solutions were taken immediately after mixing and at 30 and 60 minutes.  MHA- and MEEE-capped AuNPs were incubated with 3 mg/mL BSA at 105 mM NaCl at pH 7.4 for 90 minutes at 37 °C.  UV-visible absorbance spectra of the BSA-AuNP conjugate solutions were taken immediately after mixing and at 30, 60, and 90 minutes.  MHA-capped, MEEE-capped, and mixed-ligand AuNPs synthesized for these studies were incubated at room temperature with 0.44 mg/mL BSA in 105 mM NaCl at pH 7.4.  UV-visible absorbance spectra were taken immediately after mixing and at 5, 10, 15, 20, 30, 45, 60, and 90 minutes.

*BSA-AuNP Binding Constant Measurements by Fluorescence Titration*

BSA (0.44 mg/mL) was incubated with AuNPs in varying concentrations from 0 to 20 nM in 105 mM aqueous NaCl at pH 7.4 for 90 minutes at room temperature.  Sample

tubes and BSA solution were kept covered in foil at all times, lid removal was kept as brief as possible, and work was performed in a low-light environment.

After 90 minutes of incubation, fluorescence spectroscopy was performed with excitation at 280 nm and emission detected from 300 to 525 nm. The quartz cuvette was rinsed once with ethanol and twice with MilliQ water between each sample.

Emission intensity at 350 nm was used to determine fluorescence ratios ($F_0/F$). Stern-Volmer plots were created by plotting emission in the absence of AuNPs ($F_0$) over emission (F) vs. AuNP concentration. Hill plots were created by plotting the log of (($F_0$-F)/F-$F_{sat}$)), where $F_{sat}$ is fluorescence at saturation, vs. the log of AuNP concentration.

*Qualitative Assessment of BSA Binding to AuNPs*

Triplicate samples of 5 nM AuNPs were incubated with 0.25 mg/mL BSA for 90 minutes at room temperature in 105 mM NaCl at pH 7.4. Triplicate samples were also prepared in the same manner except for addition of MilliQ water instead of BSA. After incubation, UV-visible absorbance spectroscopy was performed for each sample. The absorbance spectra of AuNPs in water, AuNPs dispersed in saline, and AuNPs conjugated to BSA in saline were then compared.

*Bradford Assay*

Triplicate samples of 5 nM AuNPs were incubated with 0.25 mg/mL BSA for 90 minutes at room temperature in 105 mM NaCl at pH 7.4. Three negative control samples were also prepared in the same manner with MilliQ water replacing the

20

equivalent volume of AuNP solution.  After incubation, the samples were centrifuged at 16,000 g for 90 minutes and the supernatant was removed via autopipette.  A 20 μL aliquot of supernatant from each sample was removed and used to perform a Bradford protein assay.  UV-visible absorbance spectra of the remaining supernatants were taken as well.  Calibration standards were prepared from the same 10 mg/mL BSA stock solution as was used to prepare the above samples, at concentrations of 0, 125, 250, 500, 750, and 1,000 μg/mL.

20 μL of standards and samples were added to 800 μL of MilliQ water and 200 μL of Bradford reagent (Coomassie Brilliant Blue) each and incubated for 5 minutes at room temperature prior to performing UV-visible absorbance spectroscopy.  Absorbance spectra were obtained from 200-900 nm on an Agilent 8543 UV-Visible Spectroscopy System.  All spectra were obtained within one hour of incubation.  Absorbance at 595 nm was used to quantify the albumin content of all standards and samples.

CHAPTER IV

RESULTS AND DISCUSSION

*AuNP Characterization by UV-Visible Absorbance Spectroscopy*

To adequately compare the effects of different surface chemistries on BSA

adsorption, it was necessary to synthesize AuNPs with similar core diameters.  When the

core consists of gold, UV-visible absorbance spectroscopy can be used to characterize

core diameter ($d_{core}$) using the Haiss method.[7]  The ratio of absorbance at the plasmon

peak ($A_{spr}$) and absorbance at 450 nm ($A_{450}$) give the $d_{core}$ in accordance with the

exponential equation:

$$d = \exp(3.00(A_{spr}/A_{450}) - 2.20) \tag{1}$$

Applying this to the UV-visible absorbance spectra given in Figure 2, average core

diameters were found to be 4.34 nm for the MHA-capped AuNPs, 4.95 nm for the MEEE-

capped AuNPs, and 4.54 nm for the mixed-ligand AuNPs.  Throughout the course of the

study, AuNP core size was consistently verified by absorbance analysis to ensure that

particle size remained consistent in each of the experiments.

*AuNP Size Determination by TEM*

Confirmation of AuNP size was desired, and so AuNP sample TEM images were

analyzed at CAMCOR (University of Oregon) to confirm the average size provided by the

absorbance spectroscopy analysis (Figure 3). TEM images suggest that the AuNP core
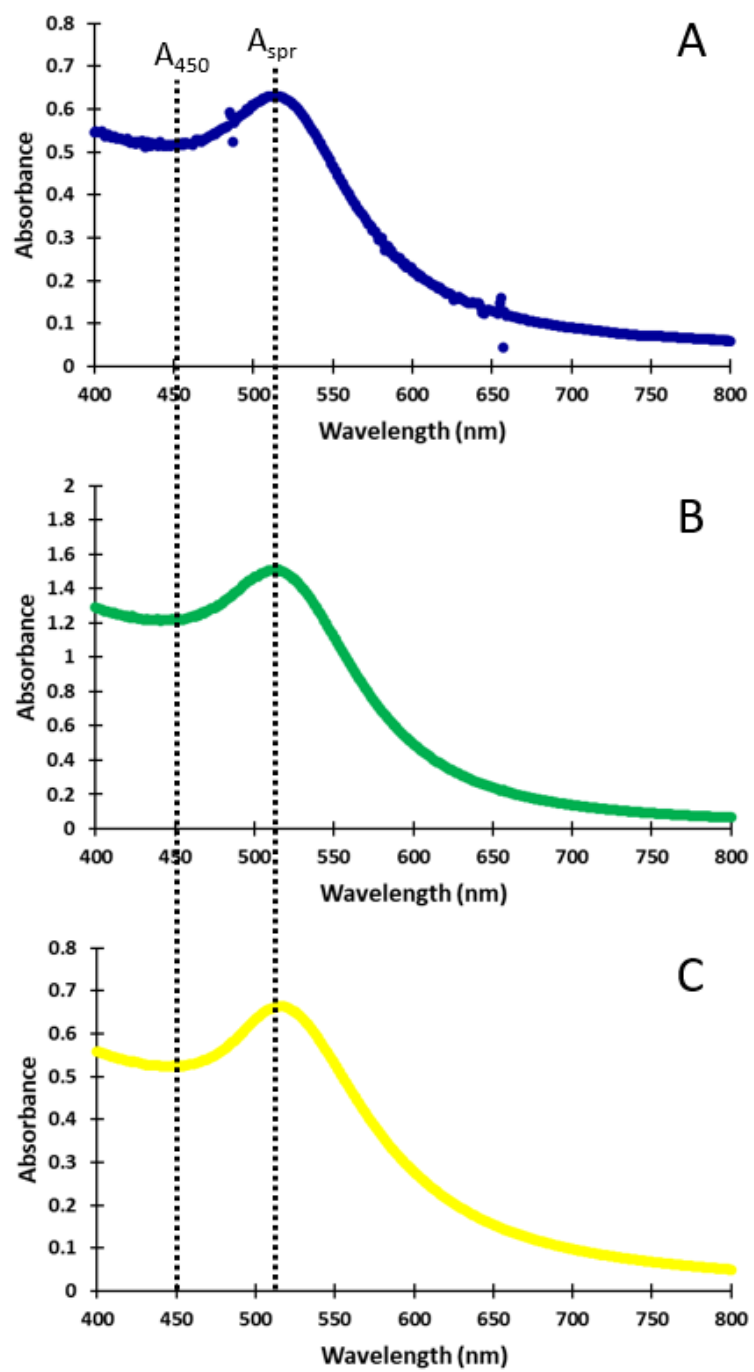
Figure 2. UV-visible absorbance spectra of synthesized and purified A. MHA-capped AuNPs, B. mixed-ligand AuNPs, and C. MEEE-capped AuNPs. Absorbance at 450 nm and at plasmon peaks are marked by dashed lines.

core sizes are consistent with the average diameter provided by the Haiss model, measuring 4.0 ± 1.4 nm (MEEE-capped AuNPs, n = 57), 5.2 ± 1.2 nm (Mixed-ligand AuNPs, n = 162), and approximately 5 nm (MHA-capped AuNPs, which were too aggregated on the grid to measure with ImageJ software).
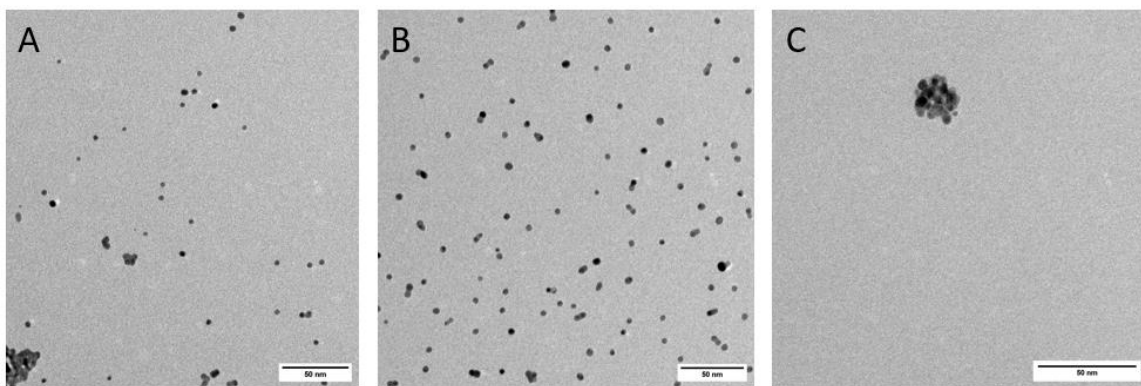


Figure 3. TEM images of A. MEEE-capped AuNPs (4.0 ± 1.4 nm, n = 57), B. Mixed-ligand AuNPs (5.2 ± 1.2 nm, n = 162), and C. MHA-capped AuNPs (too aggregated on grid to measure).

*Determination of Surface Ligand Composition by $^1$H-NMR*

To ensure that the AuNPs were synthesized with the desired surface chemistries, $^1$H-NMR spectroscopy was performed on the library of AuNPs. Figure 4 shows the $^1$H-NMR spectra of the MEEE-capped AuNPs, the MHA-capped AuNPs, and the mixed-ligand AuNPs. Peaks characteristic of pure MHA include a peak near 1.4 ppm (the $CH_2$ of the hexanoic acid alkyl chain) and a peak near 2.2 ppm ($CH_2$ α to the carbonyl carbon). MEEE shows a characteristic peak near 3.8 ppm as a result of the $CH_2$ between oxygen atoms. The spectrum of the mixed-ligand AuNPs exhibits peaks at each of these locations, showing the successful mixing of ligands on the surface of the AuNPs.

When integrated, the ratio of ligands is approximately 75:25 MEEE to MHA, quite different from the 90:10 ratio used during synthesis. Pre-digest ^{1}H-NMR spectra of the AuNPs and example spectra of the pure ligands are included in the Appendix (Figures 15-18).
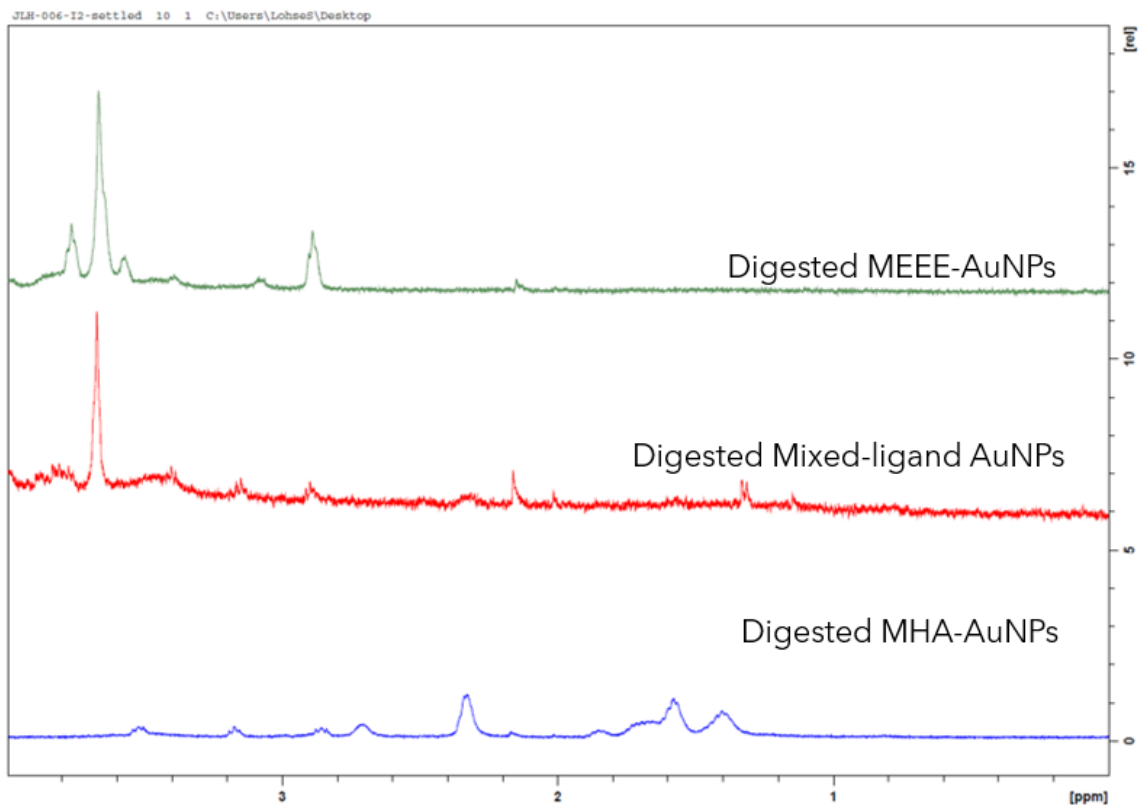


Figure 4. ^{1}H-NMR spectra (400 MHz) of diiodide-digested MEEE-capped, MHA-capped, and mixed-ligand AuNPs in deuterium oxide ($D_2O$).

*Stability Studies*

It was important to verify that the AuNPs could withstand reaction conditions (an ionic strength nearing that of physiological saline) for these studies without aggregation. The shape of the plasmon peak as it appears in the UV-visible absorbance

spectra (typically λ ~520 nm) reflects the stability of AuNPs.  If aggregation occurs the

peak shifts to the right and broadens, resulting in a higher baseline between the peak

and 800 nm.  Comparisons of spectra over time or under varying conditions provides a

picture of any aggregation or agglomeration that may take place.  In the first stability

trials, the AuNPs were incubated at 105 mM NaCl in either 30 mg/mL or 60 mg/mL BSA

to simulate the NP dispersion in a physiological environment.

The UV-visible absorbance spectra of MEEE-capped AuNPs in varying

concentrations of NaCl show a stable plasmon peak, indicating that the AuNPs remain

dispersed in solution without aggregation (Figure 5).

The spectra of the MHA-capped AuNPs, however, show that the peak shifts to a

higher wavelength at higher concentrations of NaCl, and at the highest concentration

(100 mM) there is also significant broadening (Figure 6).  The aggregation indicated by

this shift is likely a result of the negatively charged MHA ligands interacting with the

higher ionic strength environment.  A comparison of the same sample of MHA-capped

AuNPs in 100 mM NaCl over time shows that the shift and broadening of the plasmon

peak occur immediately after mixing (Figure 7).

When incubated with 30 mg/mL or 60 mg/mL BSA, both MHA- and MEEE-capped

AuNPs appeared stable over a 60-minute time period despite the presence of 105 mM

NaCl.  A representative example is shown in Figure 8 and additional spectra can be
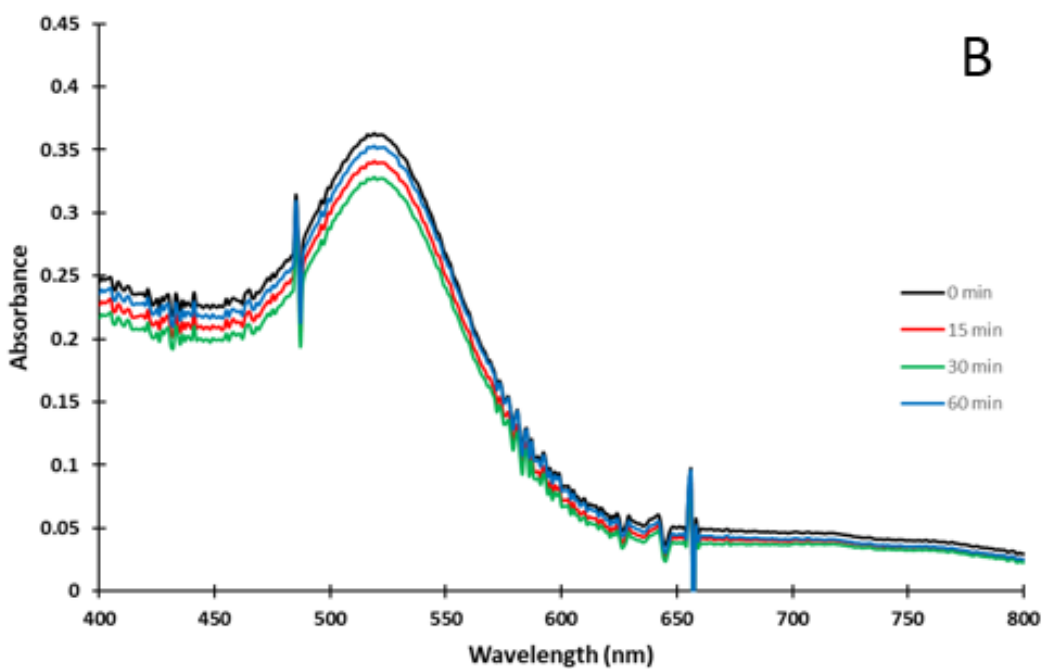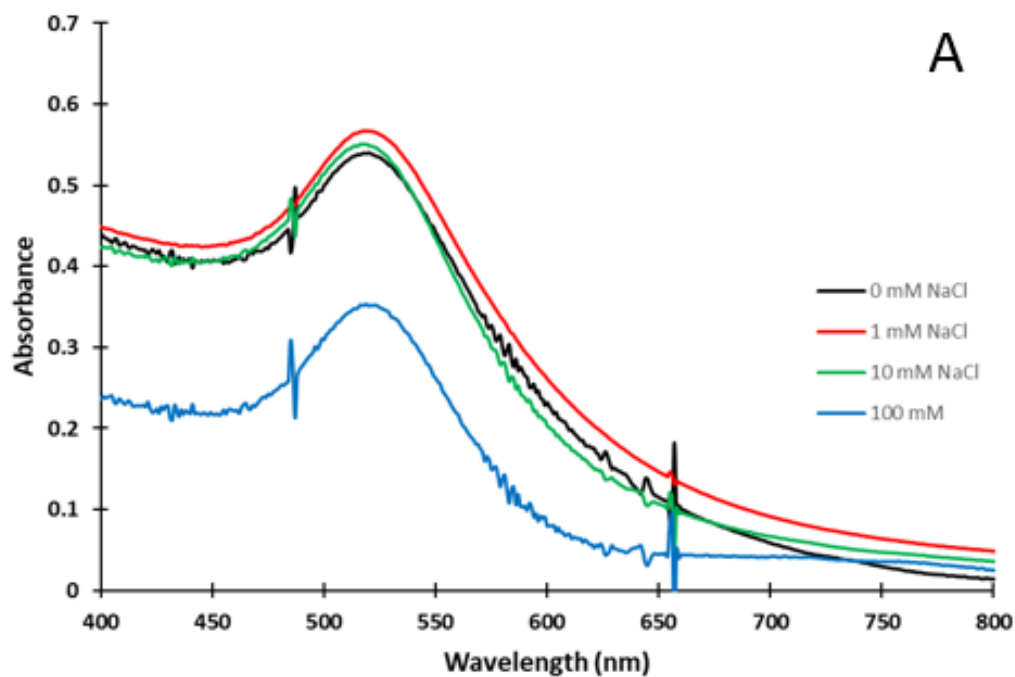
Figure 5. A. NaCl concentration-dependent UV-visible absorbance spectra of MEEE-capped AuNPs at pH 7.4 after 60 minutes of incubation at 37 °C. B. Time-dependent UV-visible absorbance spectra of MEEE-capped AuNPs incubated in 100 mM NaCl at pH 7.4 over 60 minutes of incubation at 37 °C.
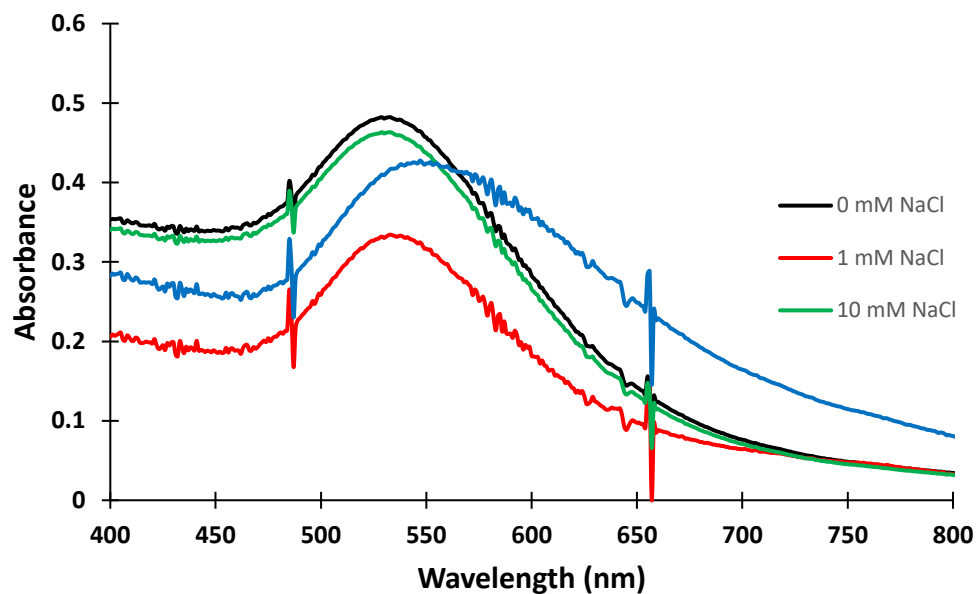
Figure 6. NaCl concentration-dependent UV-visible absorbance spectra of MHA-capped AuNPs at pH 7.4 after 60 minutes of incubation at 37 °C.
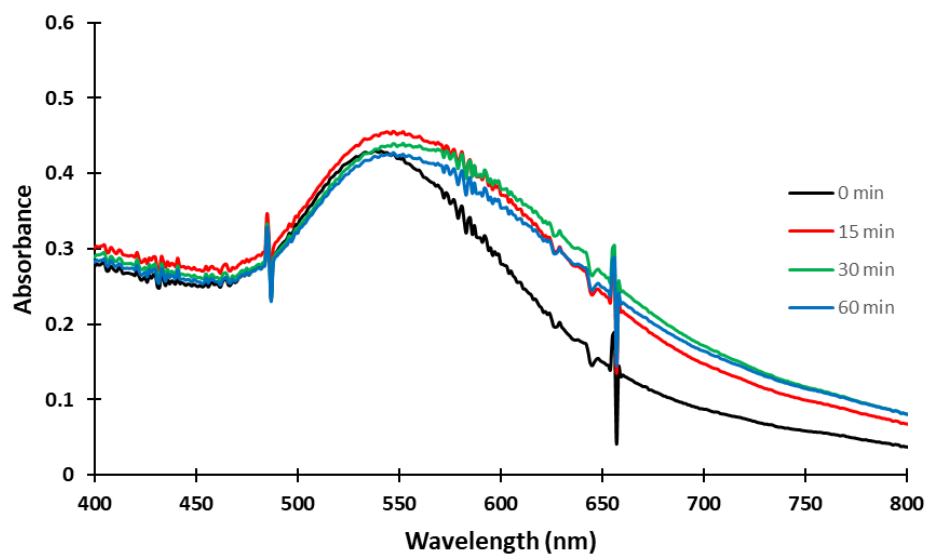


Figure 7. Time-dependent UV-visible absorbance spectra of MHA-capped AuNPs incubated in 100 mM NaCl at pH 7.4 from 0 to 60 minutes of incubation at 37 °C.

found in the Appendix (Figures A5-A12).  It is likely that the protein corona formed by the BSA protects the MHA-capped AuNPs against aggregation.

While physiological concentrations of albumin and serum proteins are in the 30-50 mg/mL and 60-80 mg/mL range respectively, much lower concentrations of BSA were needed for the Bradford assay and fluorescence titration studies.  As a result, the same qualitative stability studies were repeated at lower BSA concentrations (3 mg/mL) to assess the AuNPs' resistance to aggregation in solutions with a lower BSA concentration.

MHA- and MEEE-capped AuNPs incubated with 3 mg/mL BSA at 37 °C in 105 mM NaCl at pH 7.4 remained stable over 90 minutes.  This stability persisted when BSA concentration was reduced to 0.44 mg/mL and incubation took place at room temperature for three hours (Figure 9), with minimal shift in plasmon peak location and no peak broadening (see Appendix, Figures A13-A15).

In each trial equilibrium seems to be established almost immediately based on the absorbance spectra, but 90-minutes was selected as the optimum incubation time for the remaining studies as some published studies indicated longer times were necessary to achieve a dynamic equilibrium, and that the necessary time varied with different AuNP physiochemical properties.[9,15]

*Determination of BSA-AuNP Binding Constant Measurements by Fluorescence Titration*

Once the AuNPs were characterized, studies were undertaken to investigate their interactions with BSA, and the binding affinity of BSA for each AuNP was a critical
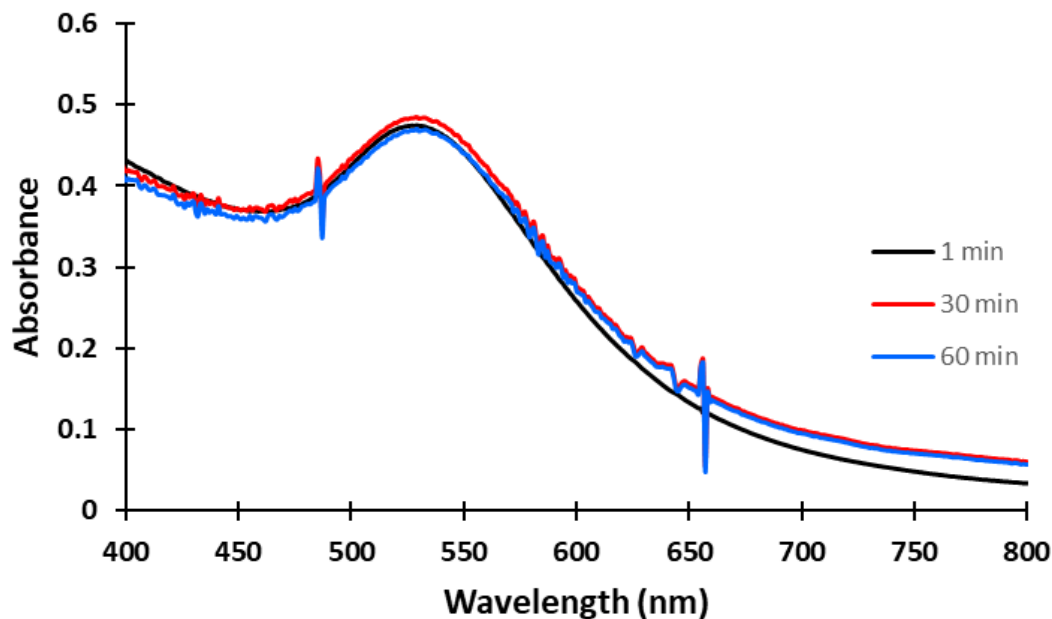
Figure 8. Time-dependent UV-visible absorbance spectra of MHA-capped AuNPs in 30 mg/mL BSA and 105 mM NaCl at pH 7.4 from 0 to 60 minutes of incubation at 37 °C.

component of this investigation.  To determine the binding affinity constant of BSA for the different AuNP surface chemistries, a fluorescence titration approach was used to generate a Stern-Volmer plot which would yield a binding constant ($K_a$) and a measure of cooperative binding between the AuNPs and BSA (via a Hill plot).

Fluorescence spectra of aqueous BSA solutions with increasing AuNP concentrations are shown in Figure 10.  The fluorescence spectra of BSA with varying concentrations of AuNPs show that as AuNP concentration increases from 0 to 3 nM, fluorescence decreases as a result of the quenching of the fluorescence by interaction of the excited BSA electrons with the electron cloud of the AuNPs.  Fluorescence intensity
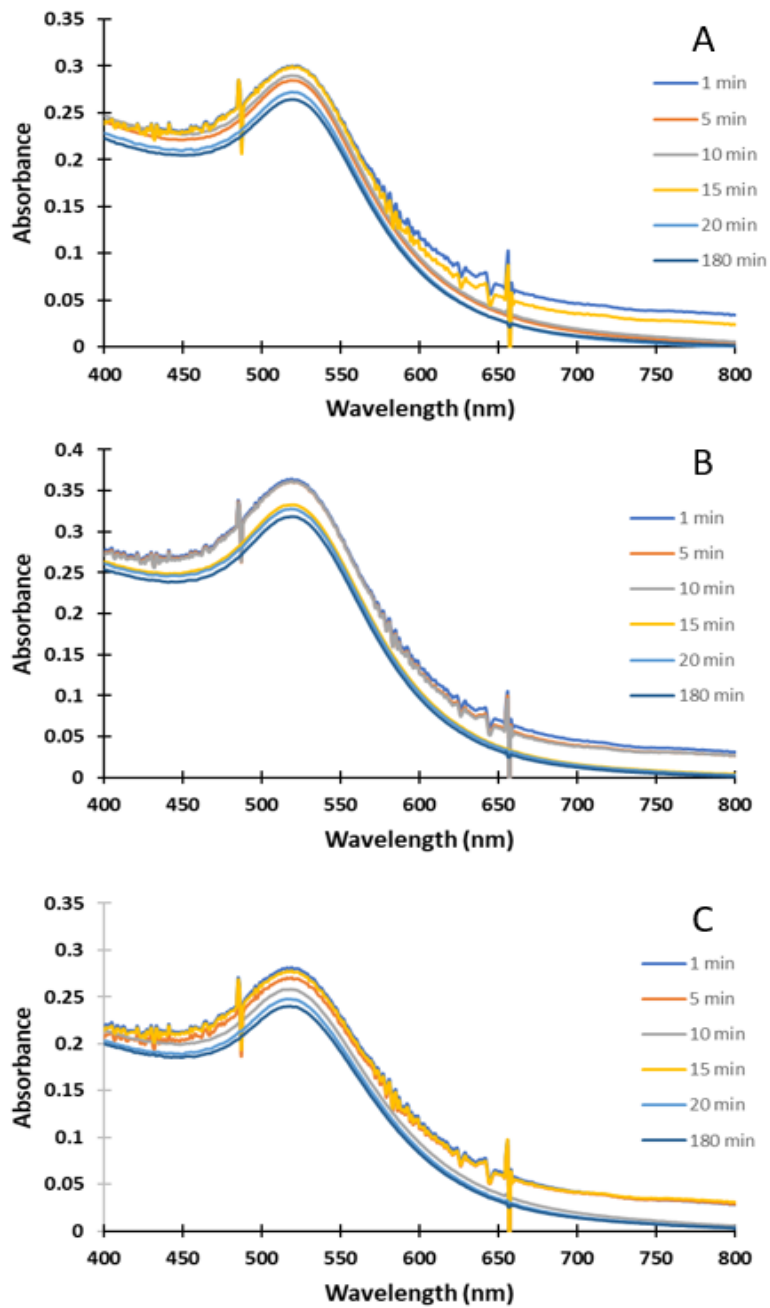
Figure 9. UV-visible absorbance spectra of A. MHA-capped AuNPs, B. Mixed-ligand AuNPs, and C. MEEE-caped AuNPs, each in 0.44 mg/mL BSA and 105 mM NaCl at pH 7.4 over 180 minutes of incubation at room temperature.

at 350 nm was used for performing data analysis as peak height occurred near this wavelength in all cases.

The loss of BSA's intrinsic fluorescence due to quenching is related to quencher concentration [Q] (in this case, [AuNP]) by the Stern-Volmer equation:

$$F_0/F = 1 + K_{SV}[Q] \tag{2}$$

where $F_0$ is the fluorescence signal with no quencher present, F is the fluorescence signal with the quencher present, and $K_{SV}$ is the Stern-Volmer constant.  Stern-Volmer plots were constructed for each AuNP type (Figure 11).

When quenching is static, that is, when the fluorophore and quencher form a stable complex, $K_{SV}$ is equal to the dissociation constant.[9]  Static quenching was expected, as the formation of the PC is stable, and this is verified by the linear relationship that is evident in the Stern-Volmer plots.

Ka for MHA, MEEE, and mixed-ligand AuNPs were 0.47 ± 0.02 nM-1, 0.40 ± 0.02 nM-1, and 0.48 ± 0.02 nM-1, respectively, indicating that the affinity of BSA for both MHA-capped and mixed-ligand AuNPs is higher than that for MEEE-capped AuNPs.  The difference between MHA and MEEE-capped and between mixed-ligand and MEEE-capped AuNPs was found to be statistically significant at the 95% confidence interval (two-tailed *t*-test, n = 3), whereas the difference between the mixed-ligand and MHA-capped AuNPs was not.  Literature values for NP $K_a$s vary depending on NP
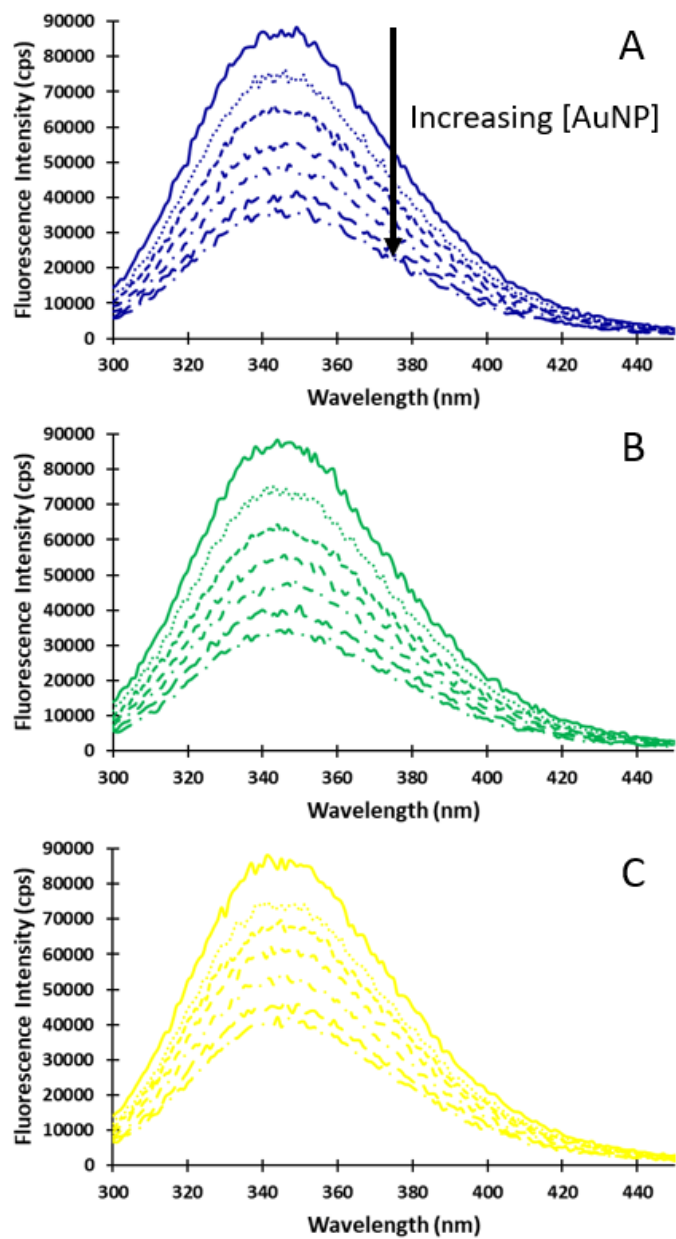
Figure 10. Fluorescence emissions spectra of 0.44 mg/mL BSA incubated for 90 minutes at room temperature in pH 7.4 105 mM NaCl with 0 to 3 nM concentrations of A. MHA-capped AuNPs, B. Mixed-ligand AuNPs, and C. MEEE-capped AuNPs. Excitation beam was set at 280 nm and emission data at 350 nm was used for Stern-Volmer and Hill plots.

characteristics, ranging for instance from 2.8 to 27.5 $nM^{-1}$ depending on size and shape

in one study of gold nanorods and AuNPs of 20 nm in diameter, so these values are not

unexpected.[9]

Fluorescence titration can also be used to determine if the binding of proteins

onto the nanoparticle is cooperative or not using a Hill plot.  When the log of the ratio of

$(F_0-F)/(F-F_{sat})$, where $F_{sat}$ is the minimum fluorescence emitted due to saturation of the

proteins with nanoparticles, is plotted against the log of nanoparticle concentration, a

linear regression can be applied.  The slope of this line determines cooperativity:  If the

slope is <1, the presence of a bound protein molecule decreases the affinity of

additional proteins for the nanoparticle, if the slope >1, it increases the affinity, and if

the slope is equal to 1, there is no effect in the affinity of additional protein molecules

for the nanoparticle.  Hill plots can be seen in Figure 12, and in all cases, *n* was greater

than 1, indicating cooperative binding of BSA molecules to the AuNP surface.

*Qualitative Assessment of BSA Binding to AuNPs*

While the fluorescence studies assessed the behavior of BSA in the presence of

AuNPs, it was also desirable to determine how the presence of BSA impacted the

behavior of the AuNPs.  Absorbance spectra for MEEE-capped, MHA-capped, and mixed-

ligand AuNPs in NaCl and in 0.25 mg/mL BSA in NaCl are shown in Figure 13.  The MHA-

capped AuNPs in NaCl without BSA show a raised baseline between 600 and 800 nm as

well as a decrease in peak intensity.  The mixed-ligand AuNPs show a marked decrease
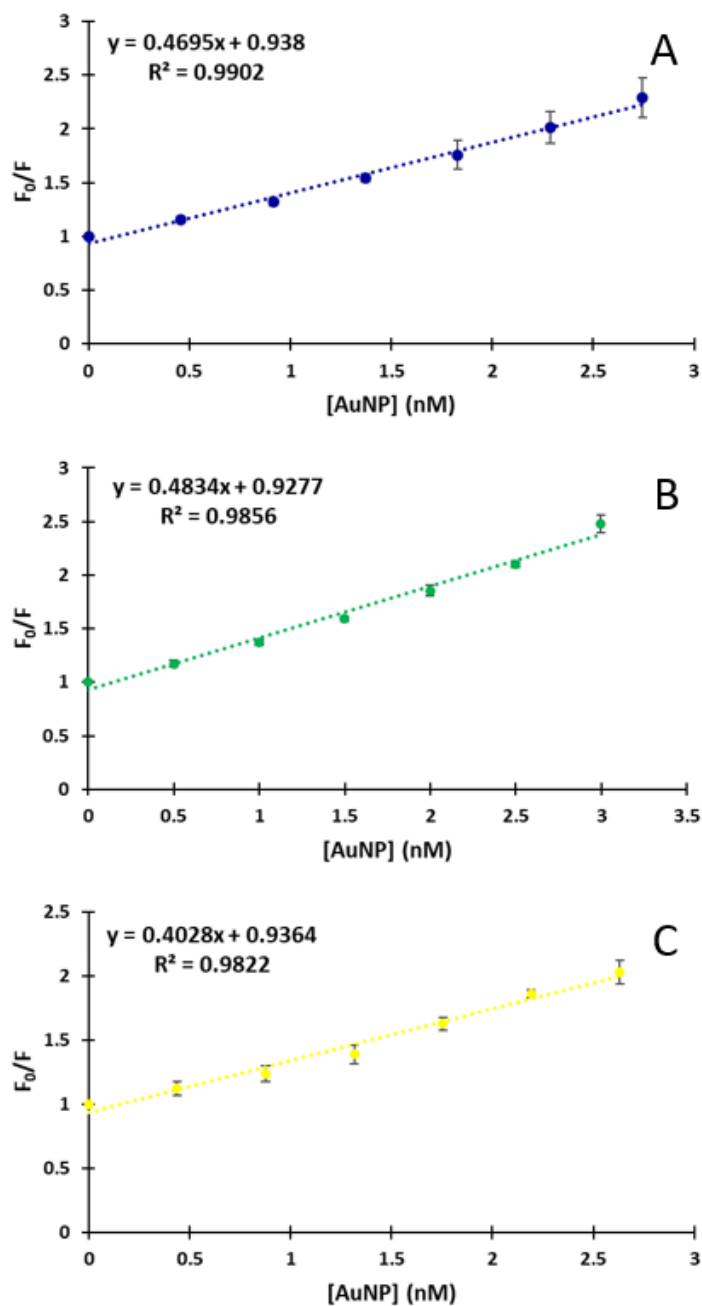
Figure 11. Stern-Volmer plots of fluorescence emission ratios at 350 nm for samples of 0.44 mg/mL BSA incubated at room temperature in 105 mM NaCl at pH 7.4 with increasing concentrations of: A. MHA-capped AuNPs, B. mixed-ligand AuNPs, and C. MEEE-capped AuNPs (n = 3). Standard deviation error bars are included but for the most part do not visibly extend beyond the data points.
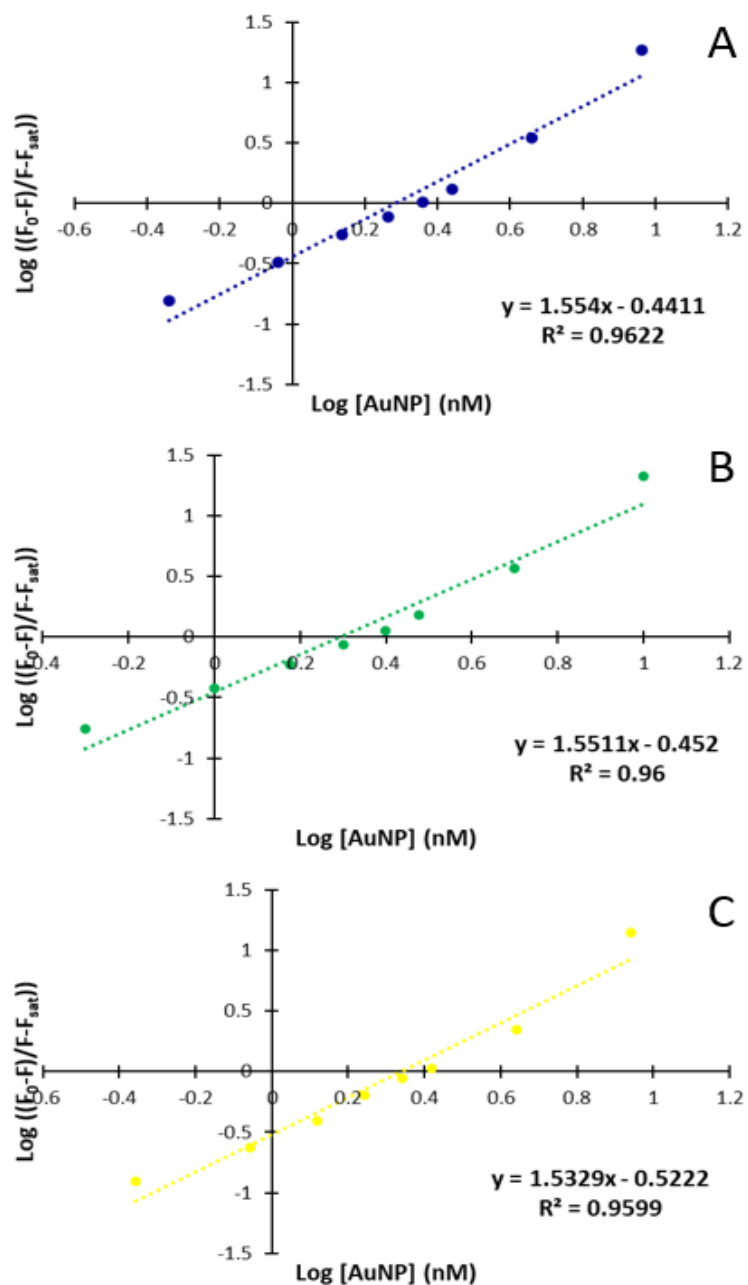
Figure 12. Hill plots of fluorescence emissions at 350 nm for samples of 0.44 mg/mL BSA incubated at room temperature in 105 mM NaCl at pH 7.4 with increasing concentrations of: A. MHA-capped AuNPs, B. mixed-ligand AuNPs, and C. MEEE-capped AuNPs (n = 3). Standard deviation error bars are included but for the most part do not visibly extend beyond the data points.

in intensity under the same conditions, and the MEEE-capped AuNPs exhibit almost

identical absorbance peaks with and without BSA.  Three characteristic features of

aggregation as seen in absorbance spectra are a red shift of the $\lambda_{max}$, a decrease in peak

intensity, and a raised baseline between 600 and 800 nm.  The absorbance spectra of

the MHA-capped AuNPs without BSA exhibit both the decreased peak intensity and the

raised baseline, but no red shift is apparent.  The mixed-ligand AuNPs exhibit only a

decreased peak intensity.

As discussed previously, aggregation of AuNPs with a negatively charged

monolayer is more pronounced in environments of higher ionic strength.  Adsorption of

BSA molecules to the AuNPs would provide steric hindrance, protecting AuNPs from

aggregation.  The spectra of the MHA-capped AuNPs, with the higher baseline and lower

peak intensity, suggests that some aggregation is present in the absence of BSA.  With

BSA present, the shape of the absorbance curve is what would be expected of non-

aggregated AuNPs.  The spectra of MEEE-capped AuNPs, on the other hand, is nearly

identical with and without BSA.  Although there is still protein adsorption with the

MEEE-capped AuNPs, these neutral AuNPs did not show aggregation in the stability

studies shown above, and thus no evidence of a protective effect of the PC is seen here.

The spectra of the mixed-ligand AuNPs is unlike either of the others.  Although peak

intensity is markedly lower (indicating a lower concentration of AuNPs), it would be hard

to conclude that aggregation had taken place without the raised baseline and red
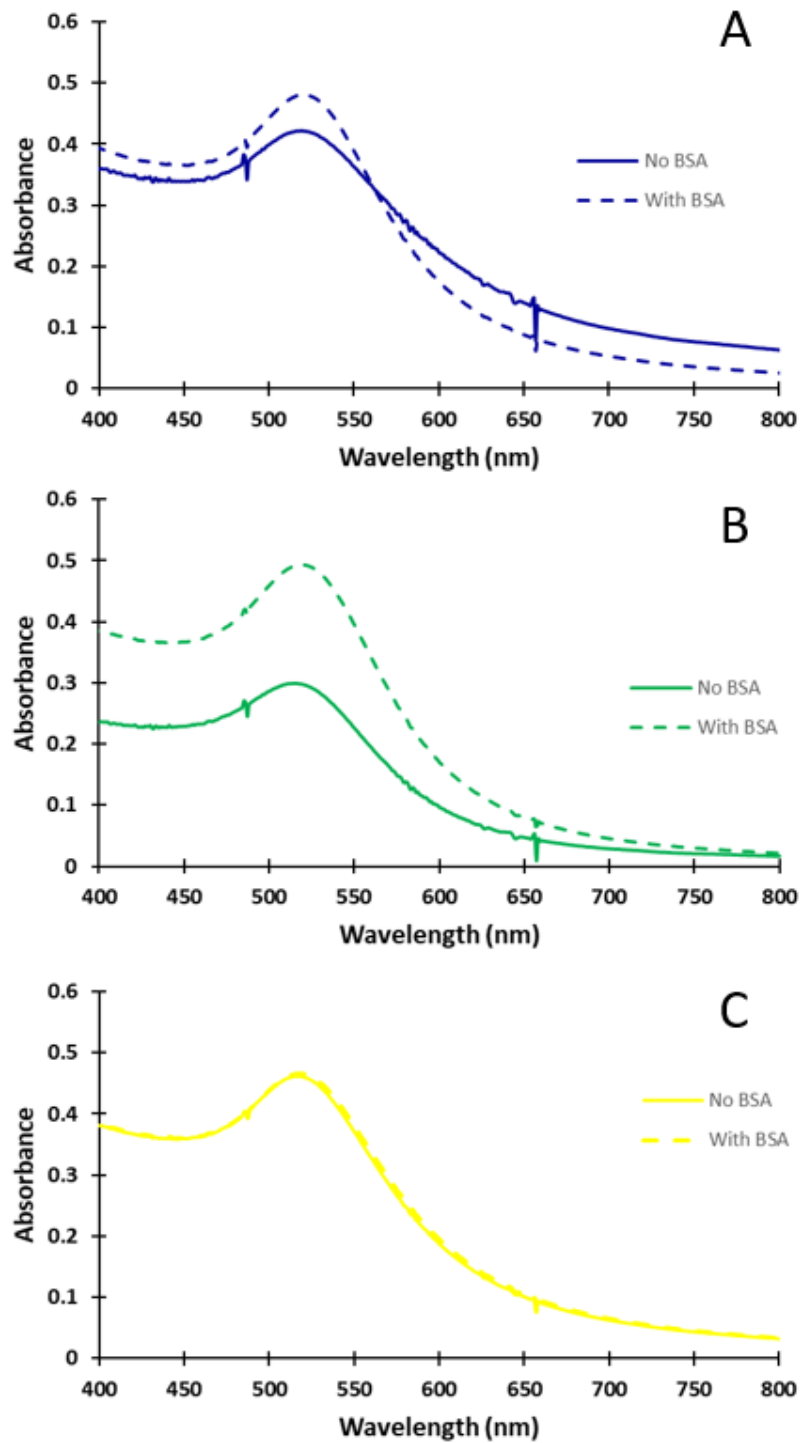
Figure 13. UV-visible absorbance spectra of A. MHA-capped, B. Mixed-ligand, and C. MEEE-capped

AuNPs in 105 mM NaCl at pH 7.4 incubated with and without .25 mg/mL BSA.

shifting that would normally be seen.  Qualitatively, the mixed-ligand AuNPs seem to

behave differently than either of the single-monolayer AuNP types, but more

investigation is required to determine what that behavior is.

*Determination of Hydrodynamic Diameter of AuNPs and BSA-AuNP complexes*

As BSA adsorbs to AuNPs, the diameter of the BSA-AuNP complex is expected to

increase.  To measure this increase, dynamic light scattering (DLS) was used.  At 5 nm in

diameter, the AuNPs studied coincided with the detection limit of the MasterSizer used,

and solution concentrations were also low.  Therefore, not all samples yielded data,

noted by "—" in Table 1.

Table 1.  Hydrodynamic Diameters of AuNPs and BSA-AuNP Complexes

| AuNP Type | $D_h$ (nm) in Water | $D_h$ (nm) in  105 mM NaCl | $D_h$ (nm) in 0.44 mg/mL BSA, NaCl |
|---|---|---|---|
| MEEE | 11 ± 11 | 8 ± 9 | — |
| Mixed-ligand | — | 5 ± 7 | 18 ± 3 |
| MHA | 8 ± 11 | — | 14 ± 10 |

Hydrodynamic diameters of AuNPs and BSA-AuNP complexes (n = 5).  Boxes with "—" denote samples for which no diameter data could be detected by the instrument. [AuNP] = 5 nM, pH = 7.4.

The hydrodynamic diameter, $D_h$, reflects the diameter of the AuNP core and the

ligand monolayer.  The measurements taken in water are in keeping with that expected

diameter.  Despite missing data points, trends can be observed.  Specifically, $D_h$ of the

BSA-AuNP complexes show a substantial increase and correlate to the adsorption of one

to two BSA molecules per AuNP.

*Quantitation of Protein Adsorption by Bradford Assay*

The differences in affinity of BSA for AuNP types should be reflected in the quantity of BSA molecules adsorbed to each AuNP.  To investigate this, a Bradford assay was undertaken.

A standard curve of absorbance at 595 nm vs. BSA concentration in μg/mL was prepared and a linear regression applied (Figure 14).  The absorbance at 595 nm of the Bradford reagent-free supernatants was subtracted from the absorbance of the Bradford samples after adjusting for supernatant dilution, and this corrected absorbance was used to calculate the BSA concentration of each sample (Table 2).  This method of background subtraction removed the contribution of residual AuNP absorbance to the absorbance values measured at 595 nm.

The UV-visible absorbance spectra of the supernatants were also used as previously described (Haiss et al.) to calculate the concentration of AuNPs remaining in the supernatant after centrifugation.  Based on the absorbance spectroscopy analysis, at the AuNP concentrations tested (5 nM), the concentrations of AuNPs remaining in the supernatant were quite high, ranging from almost 50% to almost 70%.  It is interesting to note that the mixed-ligand AuNPs were more resistant to centrifugation than the single-ligand AuNPs, and that while the size of the AuNPs remaining in the supernatant of the MHA- and MEEE-capped AuNPs was smaller than average for their samples, the size of the mixed-ligand AuNPs remaining in the supernatant were larger than average
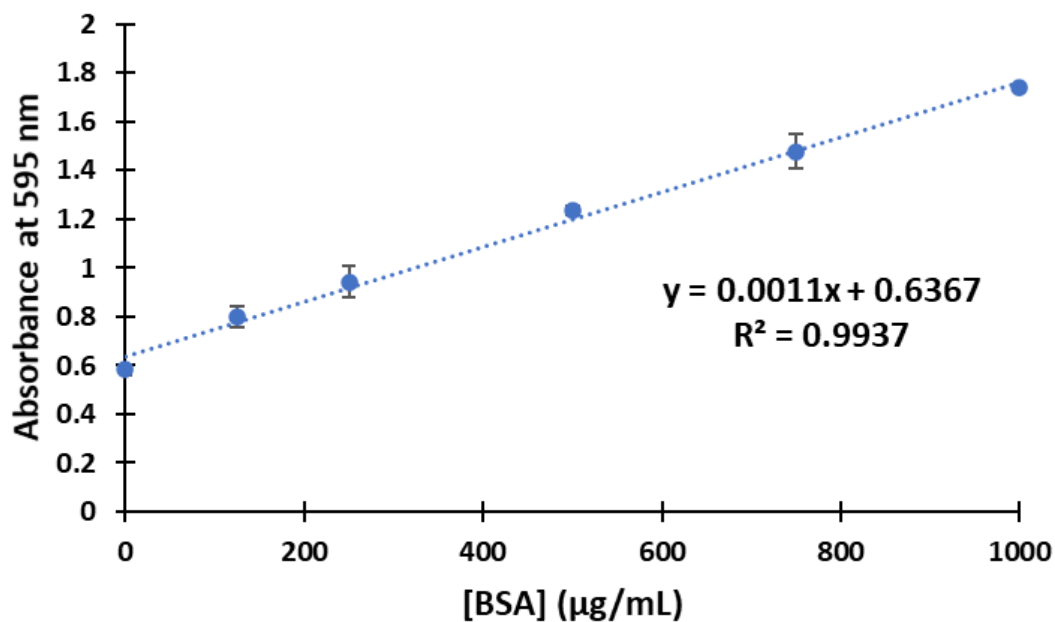
Figure 14.  Standard curve of absorbance vs. BSA concentration from 0 to 1000 µg/mL.

Table 2.  Concentration of BSA in supernatants from AuNP samples and controls.

| AuNP Type | [BSA] (µg/mL) |
|---|---|
| Mixed-ligand | 314.8 ± 0.05 |
| MHA | 335.1 ± 0.02 |
| MEEE | 333.7 ± 0.04 |
| Control (no AuNPs) | 306.4 ± 0.02 |

BSA concentration in supernatants after incubation and centrifugation (n = 3).

for its sample (see Appendix, Figures A13-A15).

Even with absorbance at 595 nm due to the AuNPs remaining in solution

accounted for, the BSA concentrations of all AuNP-treated samples, as calculated from

the Bradford assay, exceed that of the control solution.  It seems likely that the AuNPs

remaining in the supernatant cause signal enhancement.  As the absorbance at 595 nm

for the supernatant without Bradford reagent was subtracted from the absorbance of

the Bradford samples, this signal enhancement may come from interactions between

the AuNPs and the Bradford (Coomassie Blue) reagent, or from altered interactions

between the Coomassie Blue and the adsorbed BSA molecules due to conformational

changes.

Despite the spectroscopic evidence that the different AuNP surface chemistries

interact differently with BSA, the initial Bradford protein assay did not indicate any

significant difference in BSA adsorption to the different AuNP surface chemistries

tested. Specifically, due to a significant fraction of the AuNP-BSA conjugates remaining

in solution, this Bradford assay was unable to quantitate the BSA adsorbed to the AuNPs

with any certainty.

CHAPTER V

CONCLUSIONS

In this study, 5 nm AuNPs stabilized with a negatively charged functionalized thiol

(MHA-AuNPs), a neutral thiol (MEEE-AuNPs), and a mixture of the two ligands (mixed

ligand-AuNPs) were synthesized, characterized, and used to investigate the binding

interactions between the AuNPs and the model protein BSA. Characterization of the

synthesized AuNPs by UV-visible absorbance spectroscopy, EM, and DLS indicate that

the diameters of the nanoparticles fall near the target of 5 nm.  $^1$H-NMR shows that the

mixing of MEEE and MHA ligands on the AuNP surface was successful, yielding a surface

chemistry molar ratio of approximately 75:25 MEEE to MHA.  The stability of all three

AuNP-BSA conjugates surface chemistries against aggregation was verified in solutions

of very low BSA concentrations at pH 7.4 in 105 mM) NaCl (on the low end of the

physiological concentration in blood serum).  The negatively charged AuNPs (mixed-

ligand and MHA) were susceptible to mild aggregation in 105 mM NaCl in the absence of

stabilizing BSA, however.

Studies of BSA-AuNP interactions by fluorescence spectroscopy indicate that, as

expected, the affinity of BSA for the AuNPs capped with the neutrally charged MEEE

ligand is significantly less (two-tailed *t*-test, n = 3) than that for the AuNPs capped with

MHA, which is negatively charged at pH 7.4.  However, the overall binding affinity of the

MEEE-AuNPs was still comparable to that of the mixed-ligand or MHA-AuNPs (all gave $K_a$

values of 0.4-0.5 nM$^{-1}$).  The affinity of BSA for the mixed-ligand AuNPs (as measured by the $K_a$ values) and that for the MHA-capped AuNPs show no statistically significant difference (two-tailed $t$-test, n = 3), suggesting that the presence of negative charges in the surface chemistry, rather than the density of the negative charge, is the chief determiner of binding affinity.  Fluorescence studies also found that the binding of BSA to all three AuNP types studied here is cooperative.  Binding studies conducted by other groups have given varied results for binding cooperativity.[9]  Cooperativity seems to vary with NP size, shape, and surface chemistry.  As all three AuNP types here exhibit the same cooperativity, it is likely that the size of the AuNPs studied, which is approximately the same size of a BSA molecule, is the chief determiner here, allowing BSA molecules to "see" each other across the AuNP.

When AuNPs are incubated with BSA, the change in hydrodynamic diameter suggests adsorption of one to two BSA molecules per AuNP.  This would be consistent with cooperative binding between the BSA molecules, since the BSA is similar in size to the AuNPs under investigation here.  Additionally, UV-visible absorbance spectra indicate that, although the affinity of BSA for the mixed-ligand AuNPs is similar to that of BSA for MHA-capped AuNPs, the mixed-ligand AuNPs exhibit different behavior during incubation with the BSA.

Finally, while quantitation of the adsorbed BSA would be desirable, the initial attempts at the Bradford assay described herein performed did not yield definitive

44

results as sufficient separation of BSA-AuNP complexes from free BSA could not be

obtained by benchtop centrifugation alone.

REFERENCES

(1) Daniel, M.; Astruc, D. E Gold Nanoparticles: Assembly, Supramolecular Chemistry, Quantum-Size-Related Properties, and Applications toward Biology, Catalysis, and Nanotechnology. *Chem. Rev.* **2004**, *104(1),* 293-346. DOI: 10.1021/cr030698

(2) Vickers, E.T.; Garai, M.; Naghadeh, S.B.; Lindley, S.; Hibbs, J.; Xu, Q.; Zhang, J.Z. Two-Photon Photoluminescence and Photothermal Properties of Hollow Gold Nanospheres for Efficient Theranostic Applications. *J. Phys. Chem.* **2018**, *C(122),* 13304-13313. DOI: 10.1021/acs.jpcc.7b09055

(3) Mukherjee, S.; Libisch, F.; Large, N.; Neumann, O.; Brown, L.V.; Cheng, J.; Lassiter, J.B.; Carter, E.A.; Nordlander, P.; Halas, N.J. Hot Electrons Do the Impossible: Plasmon-Induced Dissociation of H2 on Au. *Nano. Lett.* **2013**, *13*, 240-247. DOI: 10.1021/nl303940z

(4) Albanese, A.; Tang, P.S.; Chan, W.C.W. The Effect of Nanoparticle Size, Shape, and Surface Chemistry on Biological Systems. *Annu. Rev. Biomed. Eng*. **2012**, *14*, 1-16. DOI: 10.1146/annurev-bioeng-071811-150124

(5) Partikel, K.; Korte, R.; Stein, N.C.; Mulac, D.; Herrmann, F.C.; Humpf, H.; Langer, K. Effect of Nanoparticle Size and PEGylation on the Protein Corona of PLGA Nanoparticles. *Eur. J. Pharm. Biopharm*. **2014**, *141*, 70-80. DOI: 10.1016/j.ejpb.2019.05.006

(6) Templeton, A.C. Wuelfing, W.P.; Murray, R.W.  Monolayer-Protected Cluster Molecules. *Acc. Chem. Res.* **2000**, *33*, 27-36. DOI: 10.1021/ar9602664

(7) Haiss, W.; Thanh, N.T.K.; Aveyard, J.; Fernig, D.G. Determination of Size and Concentration of Gold Nanoparticles from UV-Vis Spectra. *Anal. Chem*. **2007**, *79(11)*, 4215-4221. DOI: 10.1021/ac0702084

(8) Walkey, C.D.; Olsen, J.B.; Guo, H.; Emili, A.; Chan, W.C.W. Nanoparticle Size and Surface Chemistry Determine Serum Protein Adsorption and Macrophage Uptake. *J. Am. Chem. Soc*. **2012**, 134, 2139-2147. DOI: 10.1021/ja2084338

(9) Boulos, S.P.; Davis, T.A.; Yang, J.A.; Lohse, S.E.; Alkilany, A.M.; Holland, L.A.; Murphy, C.J. Nanoparticle–Protein Interactions: A Thermodynamic and Kinetic Study of the Adsorption of Bovine Serum Albumin to Gold Nanoparticle Surfaces. *Lang*. **2013**, 29, 14984–14996. DOI: 10.1021/la402920f

(10) Bradford, M.M. A Rapid and Sensitive Method for the Quantitation of Microgram Quantities of Protein Utilizing the Principle of Protein-Dye Binding. *Anal. Biochem.* **1976**, *72(1)*, 248-254. DOI: 10.1016/0003-2697(76)90527-3

(11) Murphy, C.J.; Chang, H.; Falagan-Lotsch, P.; Gole, M.T.; Hofmann, D.M.; Hoang, K.N.L.; McClain, S.M.; Meyer, S.M.; Turner, J.G.; Unnikrishnan, M.; Wu, M.; Zhang, X.; Zhang, Y.Virus-Sized Gold Nanorods: Plasmonic Particles for Biology. *Acc. Chem. Res*. **2019**, *52*, 2124-2135. DOI: 10.1021/acs.accounts.9b00288

(12) Cole, J.R.; Mirin, N.A.; Knight, M.W.; Goodrich, G.P.; Halas, N.J. Photothermal Efficiencies of Nanoshells and Nanorods for Clinical Therapeutic Applications. *J. Phys. Chem*. **2009**, *113*, 12090-12094. DOI: 10.1021/jp9003592

(13) Sokolov, K.; Follen, M.; Aaron, J.; Pavlova, I.; Malpica, A.; Lotan, R.; Richards-Kortum, R. Real-Time Vital Optical Imaging of Precancer Using Anti-Epidermal Growth Factor Receptor Antibodies Conjugated to Gold Nanoparticles. *Cancer Research*. **2003**, *62*, 1999-2004.

(14) Mahmoudi, M.; Bertrand, N.; Zope, H.; Farookhzad, O.C.  Emerging Understanding of the Protein Corona at the Nano-Bio Interfaces. *Nan. Tod.* **2016**, *11*, 817-832. DOI: dx.doi.org/10.1016/j.nantod.2016.10.005

(15) Piella, J. Bastus, N.G.; Puntes, V. Size-Dependent Protein–Nanoparticle Interactions in Citrate-Stabilized Gold Nanoparticles: The Emergence of the Protein Corona. *Bioconjugate Chem.* **2017**, 2*8*, 88-97. DOI: 10.1021/acs.bioconjchem.6b00575

(16) Wang, G.; Yan, C.; Gao, S.; Liu, Y. Surface Chemistry of Gold Nanoparticles Determines Interactions with Bovine Serum Albumin. *Mater. Sci. Eng. C.* **2019**, 103, 109856–109856. DOI: 10.1026/j.msec.2019.109856

(17) Larson, T.A.; Joshi, P.P.; Sokolov, K. Preventing Protein Adsorption and Macrophage Uptake of Gold Nanoparticles via a Hydrophobic Shield. *ACS Nano*. **2012**, *6(10)*, 9182-9190. DOI: 10.1021/nn3035155

(18) Walkey, C.D.; Olsen, J.B.; Song, F.; Liu, R.; Guo, H.; Olsen, D.W.H; Cohen, Y.; Emili, A.; Chan, W.C.W. Protein Corona Fingerprinting Predicts the Cellular Interactions of Gold and Silver Nanoparticles. *ACS Nano*. **2014**, *8(3)*, 2439-2455. DOI: 10.1021/nn406018q

(19) Zhang, Y.; Wu, J.L.Y.; Lazarovits, J.; Chan, W.C.W. An Analysis of the Binding

Function and Structural Organization of the Protein Corona. *J. Am. Chem. Soc*. **2020**,

*142,* 8827-88365. DOI: 10.1021/.0c01853

(20) Mosquera, J.; Garcia, I.' Liz-Marzan, L.M. Cellular Uptake of Nanoparticles versus

Small Molecules: A Matter of Size. *Acc. Chem. Res*. **2018**, *51*, 2305-2313. DOI:

10.1021/acs.accounts.8b00292

(21) Connor, E.E.; Mwamuka, J.; Gole, A.; Murphy, C.J.; Wyatt, M.D. Gold Nanoparticles

Are Taken Up by Human Cells but Do Not Cause Acute Cytotoxicity. *Small*. **2005**, *1(3)*,

325-327. DOI: 10.1002/smll.200400093

(22) Dominguez-Medina, S.; Kisley, L.; Tauzin, L.J.; Hoggard, A.; Shuang, B.; Indresakara,

A.S.D.S.; Chen, S.; Wang, L.; Derry, P.J.; Liopo, A.; Zubarev, E.R.; Landes, C.F.; Link, S.

Adsorption and Unfolding of a Single Protein Triggers Nanoparticle Aggregation. *ACS

Nano.* **2016**, *10*, 2103-2112. DOI: 10.1012/acsnano.5b06439

(23) Chakraborty, S.; Joshi, P.; Shanker, V.; Ansari, Z.A.; Singh, S.P.; Chakrabarti, P.

Contrasting Effect of Gold Nanoparticles and Nanorods with Different Surface

Modifications on the Structure and Activity of Bovine Serum Albumin.  *Lang.* **2011**, *27*,

7722-7731. DOI: 10.1021/la200787t

(24) Shi, X.; Li, D.; Xie, J.; Wang, S.; Wu, Z.; Chen, H.  Spectroscopic Investigation of the

Interactions Between Gold Nanoparticles and Bovine Serum Albumin. *Chi. Sci. Bull.*

**2012**, *57(10)*, 1109-1115 . DOI: 10.1007/s11434-011-4741-3

(25) Lohse, S.E; Dahl, J.A.; Hutchison, J.E. Direct Synthesis of Large Water-Soluble

Functionalized Gold Nanoparticles Using Bunte Salts as Ligand Precursors. *Lang*. **2010**,

*26(10)*, 7504-7511. DOI: 10.1021/la904306a

(26) Elliott, E.W.; Haben, P.M.; Hutchison, J.E. Subnanometer Control of Mean Core Size

during Mesofluidic Synthesis of Small (Dcore < 10 nm) Water-Soluble, Ligand-Stabilized

Gold Nanoparticles. *Lang*. **2015**, *31(43)*, 11886–11894. DOI:

10.1021/acs.langmuir.5b02419
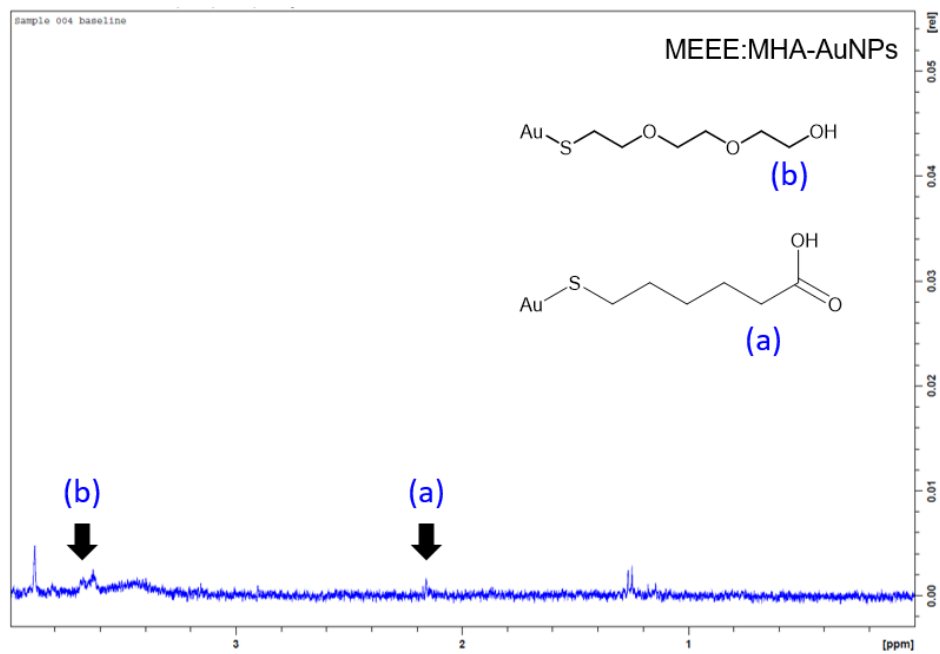
Figure A1. $^1$H-NMR spectra of mixed mixed-ligand AuNPs with characteristic peaks indicated.
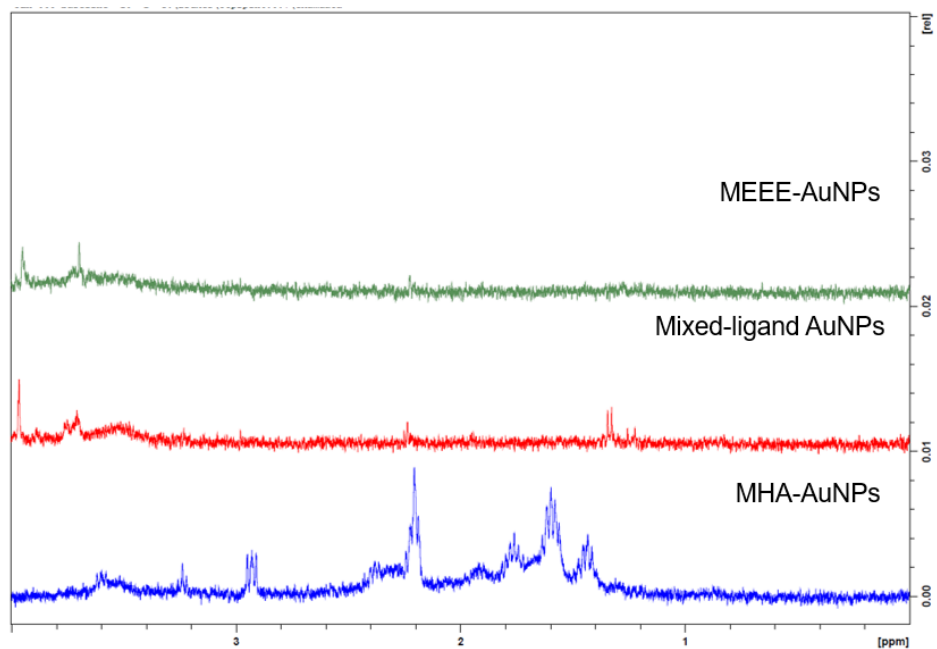


Figure A2. Pre-digest $^1$H-NMR spectra of MEEE-capped, MHA-capped, and mixed-ligand AuNPs.
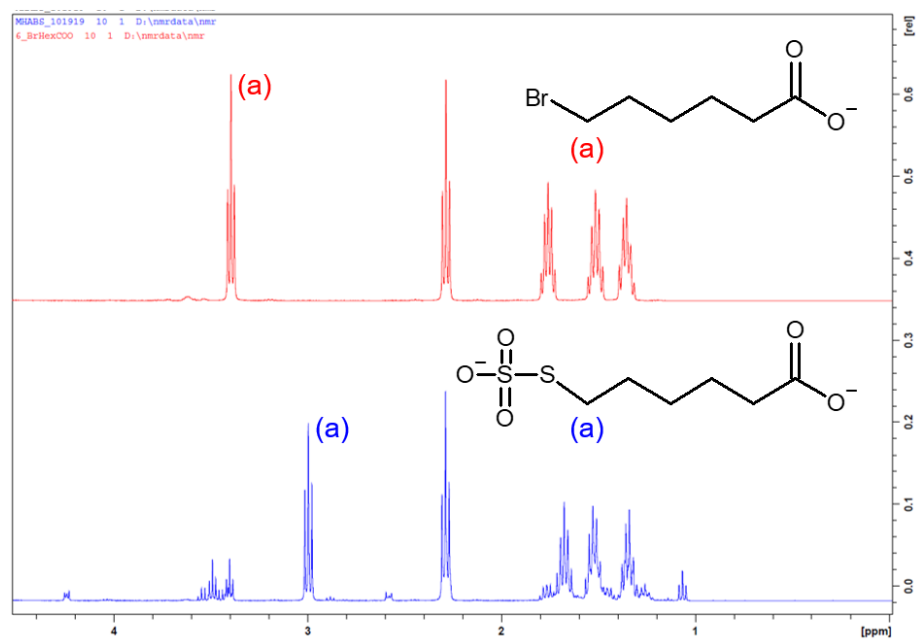
Figure A3.  Representative 1H-NMR spectra of MHA Bunte salt analog and its organohalide precursor.
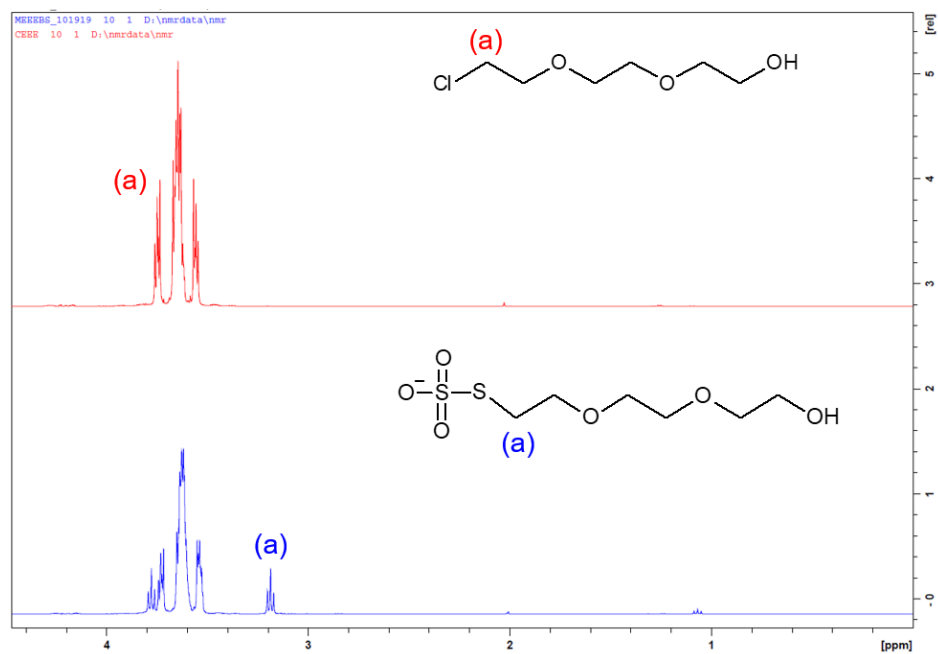


Figure A4.  Representative 1H-NMR spectra of MEEE Bunte salt analog and its organohalide precursor.
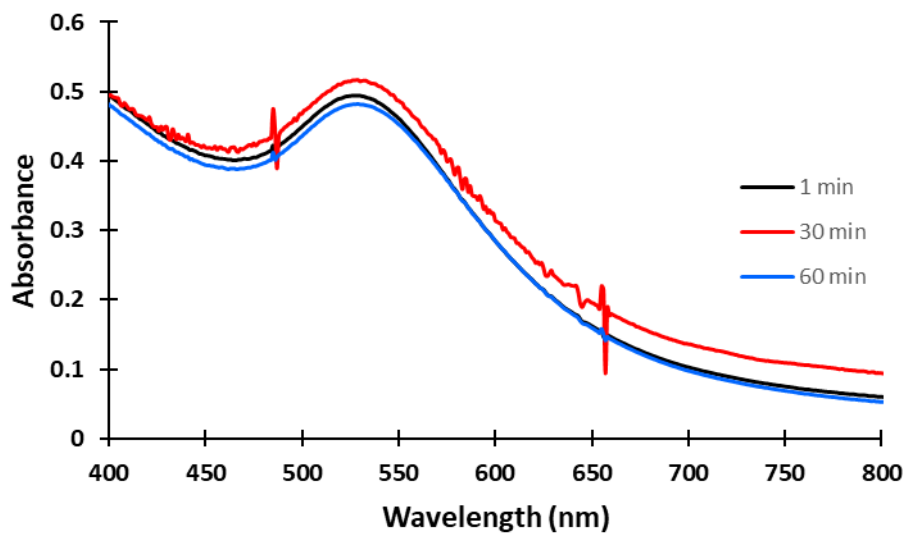
Figure A5.  Time-dependent UV-visible absorbance spectra of MHA-capped AuNPs incubated with 60 mg/mL BSA in 105 mM NaCl at pH 7.4 from 1 to 60 minutes.
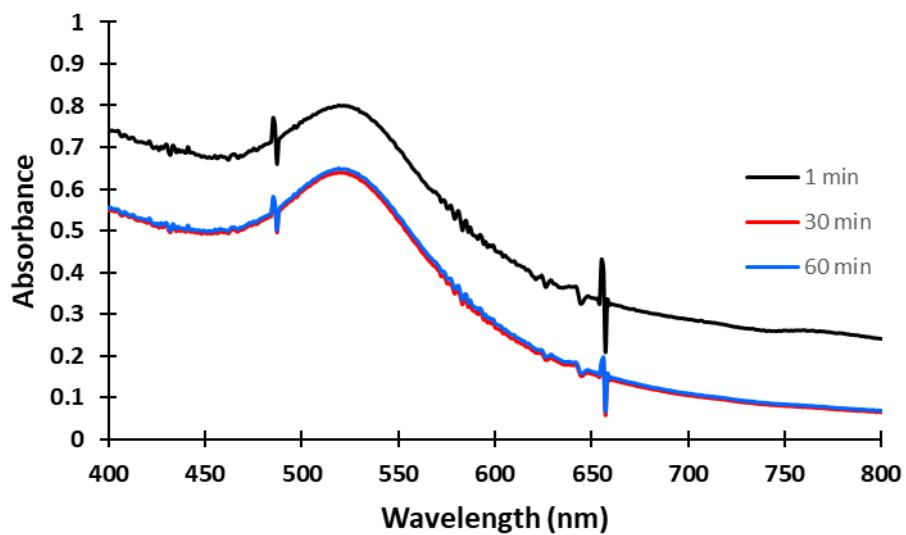


Figure A6.  Time-dependent UV-visible absorbance spectra of MEEE-capped AuNPs incubated with 30 mg/mL BSA in 105 mM NaCl at pH 7.4 from 1 to 60 minutes.
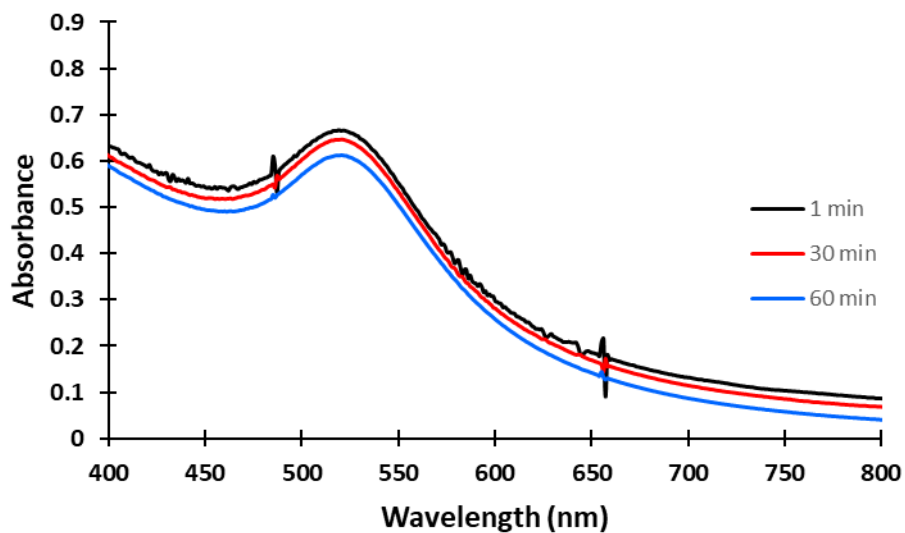
Figure A7. Time-dependent UV-visible absorbance spectra of MEEE-capped AuNPs incubated with 60 mg/mL BSA in 105 mM NaCl at pH 7.4 from 1 to 60 minutes.
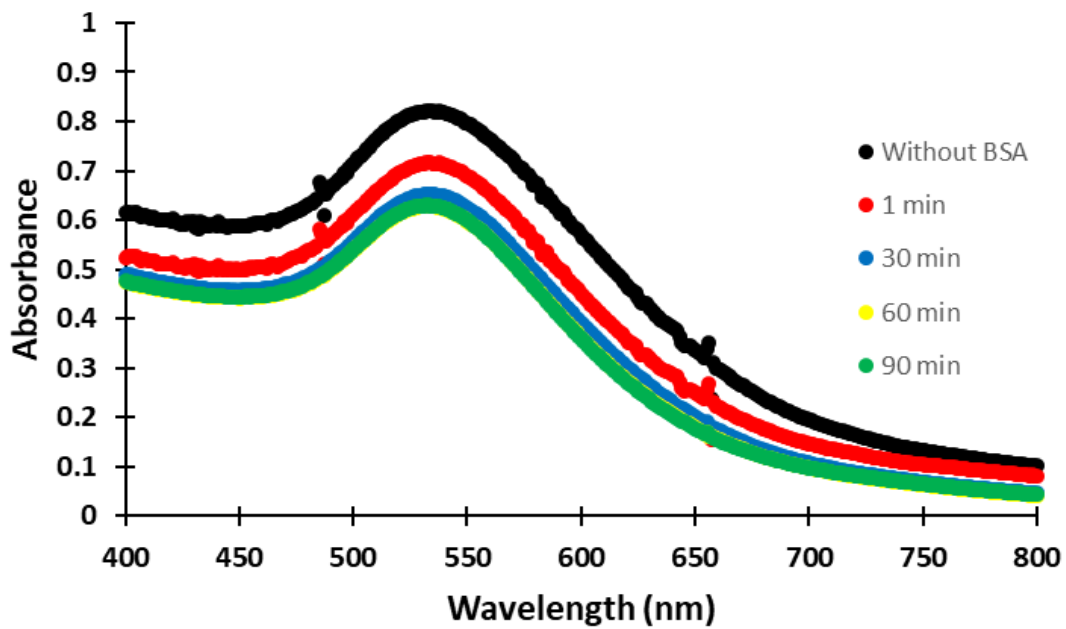


Figure A8. Time-dependent UV-visible absorbance spectra of MHA-capped AuNPs in 3 mg/mL BSA and 105 mM NaCl at pH 7.4 from 0 to 90 minutes of incubation at 37 °C.
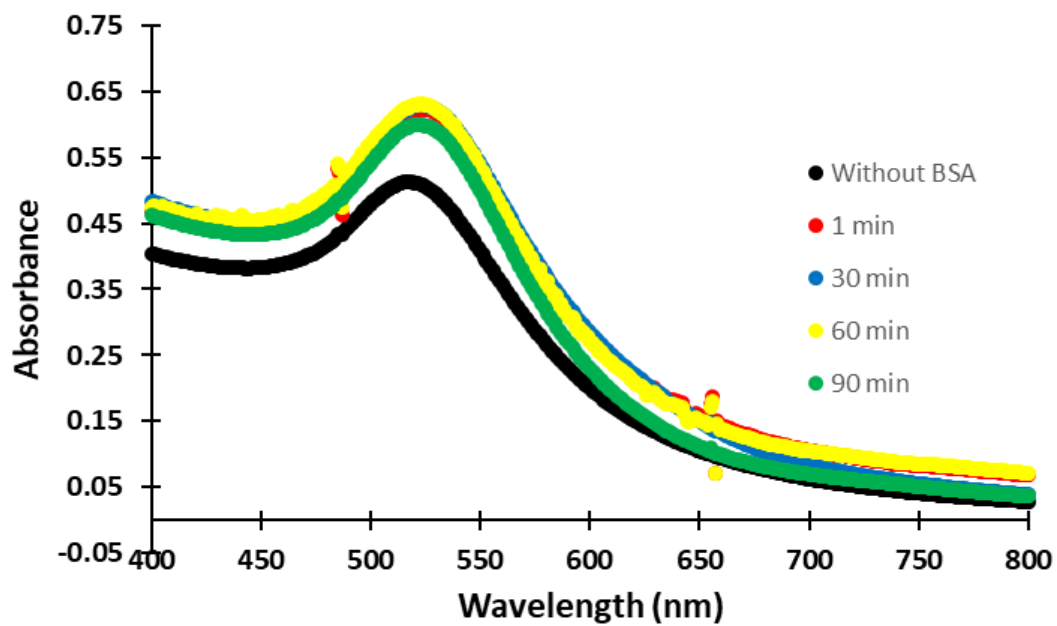
Figure A9.  Time-dependent UV-visible absorbance spectra of MEEE-capped AuNPs in 3 mg/mL BSA and

105 mM NaCl at pH 7.4 from 0 to 90 minutes of incubation at 37 °C.
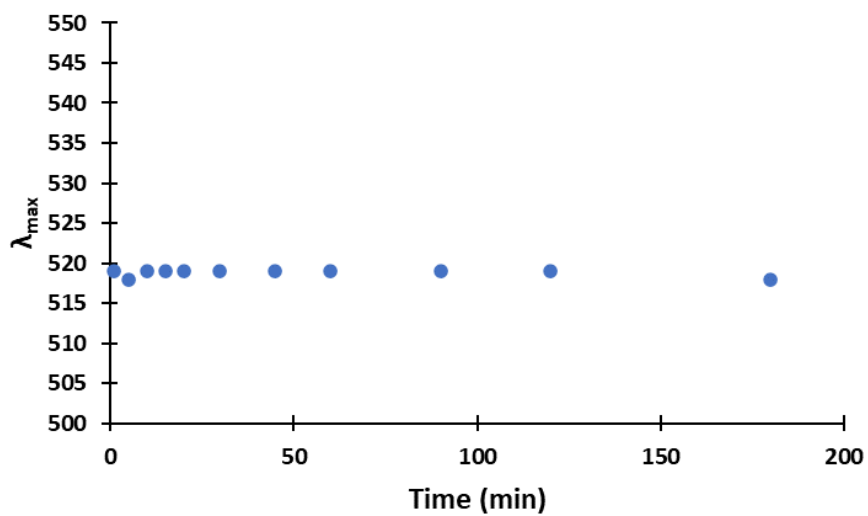


Figure A10.  Wavelength of location of the plasmon peak given by UV-visible absorbance spectroscopy of

MHA-capped AuNPs in 0.44 mg/mL BSA and 105 mM NaCl at pH 7.4 over 180 minutes of incubation at
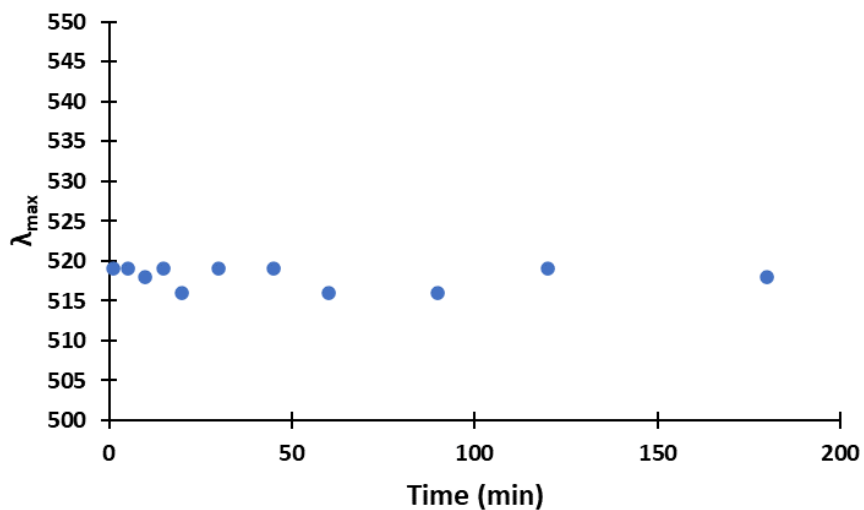
room temperature.

Figure A11.  Wavelength of location of the plasmon peak given by UV-visible absorbance spectroscopy of

MEEE-capped AuNPs in 0.44 mg/mL BSA and 105 mM NaCl at pH 7.4 over 180 minutes of incubation at
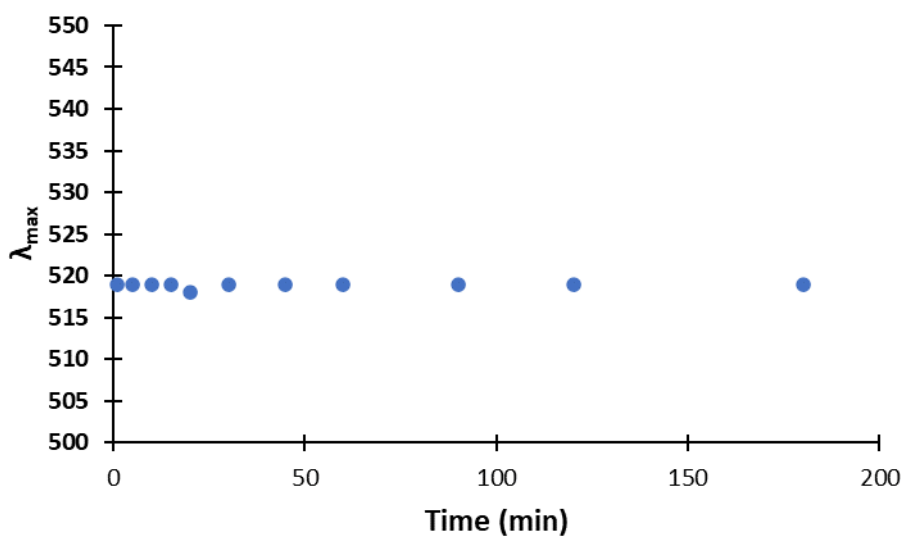
room temperature.



Figure A12.  Wavelength of location of the plasmon peak given by UV-visible absorbance spectroscopy of

mixed-ligand AuNPs in 0.44 mg/mL BSA and 105 mM NaCl at pH 7.4 over 180 minutes of incubation at

room temperature.
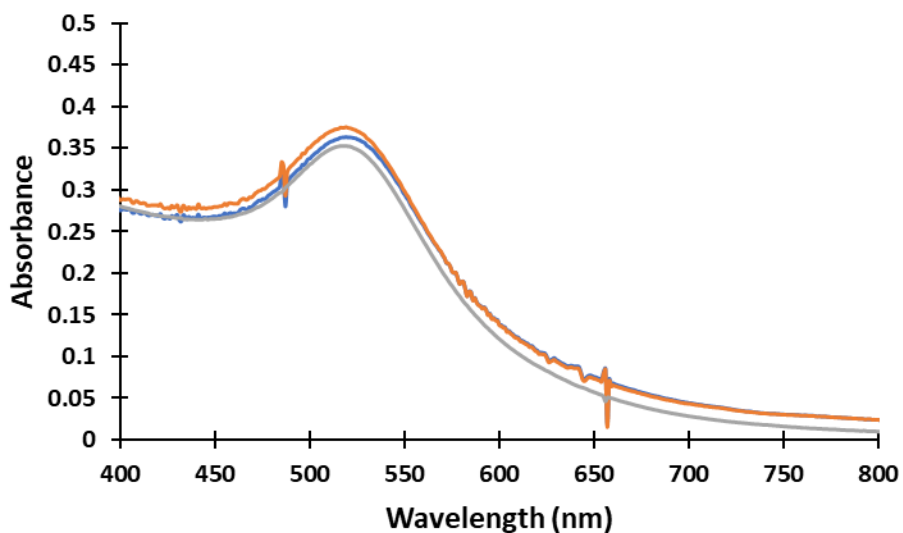
Figure A13. UV-visible absorbance spectra of supernatant remaining after centrifugation of mixed-ligand AuNPs incubated with 0.25 mg/mL BSA in 105 mM NaCl at pH 7.4. Per the Haiss method, the AuNP size was 6.1 nm and concentration was 3.37 nM.
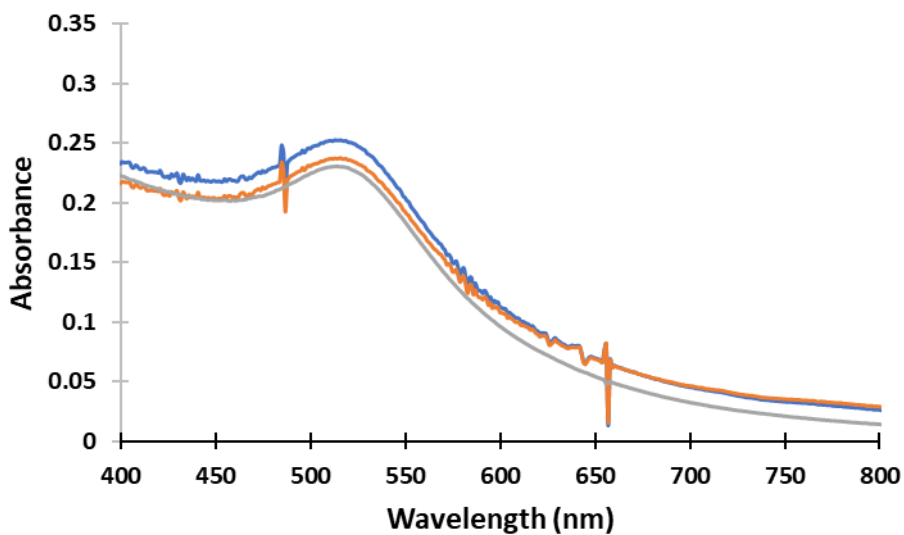


Figure A14. UV-visible absorbance spectra of supernatant remaining after centrifugation of MHA-capped AuNPs incubated with 0.25 mg/mL BSA in 105 mM NaCl at pH 7.4. Per the Haiss method, the AuNP size was 3.6 nm and concentration was 2.83 nM.
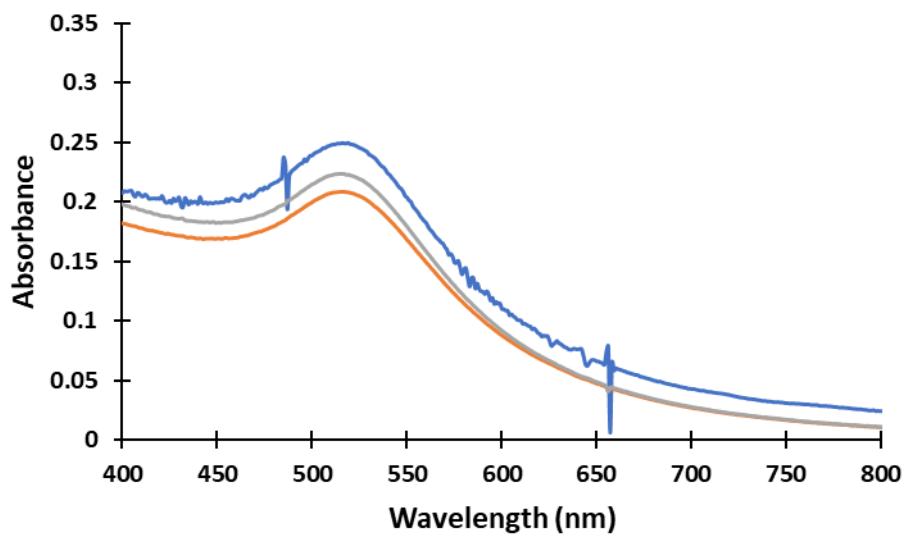
Figure A15.  UV-visible absorbance spectra of supernatant remaining after centrifugation of MEEE-capped

AuNPs incubated with 0.25 mg/mL BSA in 105 mM NaCl at pH 7.4.  Per the Haiss method, the AuNP size

was 4.5 nm and concentration was 2.44 nM.